A coiled-coil affinity-based system for the controlled release of biofunctionalized gold nanoparticles from alginate hydrogels

BioMACROMOLECULES

Article

A coiled-coil affinity-based system for the controlled release of biofunctionalized gold nanoparticles from alginate hydrogels

Audrey Roth, Frederic Murschel, Pierre-Luc Latreille, Vincent A. Martinez, Benoît Liberelle, Xavier Banquy, and Gregory De Crescenzo

Biomacromolecules, **Just Accepted Manuscript** • DOI: 10.1021/acs.biomac.9b00137 • Publication Date (Web): 05 Apr 2019

ACS Publications

is published by the American Chemical Society. 1155 Sixteenth Street N.W., Washington, DC 20036

A coiled-coil affinity-based system for the controlled release of biofunctionalized gold nanoparticles from alginate hydrogels

Audrey Roth[1], Frederic Murschel[2], Pierre-Luc Latreille[2], Vincent A. Martinez[3], Benoît Liberelle[1], Xavier Banquy[2], Gregory De Crescenzo[1]**

[1]Department of Chemical engineering, Groupe de Recherche en Sciences et Technologies Biomédicales (GRSTB), Bio-P[2] Research Unit, École Polytechnique de Montréal, Montréal, QC, Canada

[2]Canadian Research Chair in Bioinspired materials, Faculty of Pharmacy, Université de Montréal, Montréal, QC, Canada

[3]School of Physics and Astronomy, The University of Edinburgh, Peter Guthrie Tait Road, Edinburgh, EH9 3FD, UK

ABSTRACT

Affinity-based systems represent a promising solution to control the delivery of therapeutics using hydrogels. Here, we report a hybrid system that is based on the peptidic E/K coiled-coil affinity pair to mediate the release of gold nanoparticles from alginate scaffolds. On the one hand, the gold nanoparticles were functionalized with Ecoil-tagged epidermal growth factor (EGF). The bioactivity of the grafted EGF and the bioavailability of the Ecoil moiety were confirmed by EGF receptor phosphorylation assays and by capturing the functionalized nanoparticles on a Kcoil-derivatized surface, respectively. On the other hand, alginate chains were modified with azido-homoalanine Kcoil (Aha-Kcoil) by azide-alkyne click chemistry. The hybrid system was formed by dispersing NPs functionalized with Ecoil-tagged EGF in alginate hydrogels containing either 0, 10 or 20% of Kcoil-modified alginate (Alg-Kcoil). With 20% of Alg-Kcoil, the release of Ecoil-functionalized NPs was reduced by half when compared to the release of NPs without Ecoil, whereas little to no differences were noticed with either 0 or 10% of Alg-Kcoil. Differential dynamic microscopy was used to determine the diffusion coefficient of the NPs, and the results showed a decrease in the diffusion coefficient of Ecoil-functionalized NPs, when compared to bare pegylated NPs. Altogether, our data demonstrated that the E/K coiled-coil system can control the release of NPs in a high Kcoil content alginate gel, opening diverse applications in drug delivery.

KEYWORDS. Coiled-coil, affinity, diffusion, hydrogel, gold nanoparticle, differential dynamic microscopy

1. Introduction

Researchers from numerous fields strive to develop systems that allow for the controlled and efficient delivery of therapeutics, especially for long-term release. A number of complementary strategies have emerged in that endeavor; they have been applied to many types of therapeutics, from hydrophobic molecules to nucleic acids, peptides and proteins. A very popular method consists in encapsulating the therapeutic agent in polymeric micro- or nanoparticles.[1,2] Release is, in this case, governed by particle degradation and passive diffusion of the therapeutic. The encapsulation process however tends to degrade peptides and proteins and has therefore been primarily applied to small hydrophobic molecules.[3] The incorporation of the drug in a polymeric scaffold is another frequently encountered strategy, for which the release is mainly regulated by scaffold swelling and/or scaffold degradation, be it in bulk or by surface erosion, although passive diffusion can play a significant role.[4] Affinity-based delivery strategies have recently gained a lot of interest as they may offer more versatility and can promote long-term and continuous release of drugs or proteins.[3] Indeed, by incorporating a specific biological anchor in a polymeric scaffold, the molecule diffusion can be dramatically slowed down and thus release can be stretched over a long period of time.[3,5] These systems have been growing in number and variety, and show potential for an increasing number of applications.[6–10]

Most affinity-based strategies thus far have relied on naturally occurring interactions between the protein or drug of interest and one of its biological partners. Glycans such as heparin and sulfates have been widely reported as a means to sequester heparin-binding proteins within scaffolds[11], which has significantly extended the duration of protein delivery up to several days.[6,12] Similarly, complexes of β-cyclodextrins have been covalently incorporated in hydrogels to control the release

of hydrophobic low molecular weight proteins.[13] Some research groups have engineered polysaccharide fragments and peptide sequences inspired by natural biomolecules to interact more specifically with the therapeutic of interest and/or to better control its delivery.[14] For instance, Lin *et al.* were able to control the release profile of a growth factor from a poly(ethylene glycol) (PEG) hydrogel by functionalizing PEG chains with affinity binding peptides.[7] Similarly, Wang *et al*. developed a competitive affinity-based system to release multiple proteins at different timepoints of the treatment.[8] More precisely, the vascular endothelial and the platelet-derived growth factors were immobilized on polystyrene microparticles using two different aptamers and then those microparticles were dispersed in a hydrogel. Protein release could then be triggered by simple incubation of a competitive aptamer sequence. Regardless, systems based on natural interactions suffer from a lack of versatility. Indeed, most designs only suit a narrow panel of therapeutic agents, given that each drug may require its own partner and specific hydrogel characteristics. Moreover, the release profiles are dictated by the thermodynamics of the interaction, which are hardly tunable for natural partners. The advances in biomolecule design and synthesis, notably by protein engineering, may offer a way to circumvent these issues and fulfill the current need for more flexibility and finer control of spatiotemporal delivery.

Coiled-coils are a ubiquitous motif found in proteins that has been discovered more than six decades ago and has been the core subject of many scientific works. The research based on *de novo* designed coiled-coil forming peptides has led to a robust knowledge of the determinants of their interactions.[15–17] The rational design of peptide sequences that feature tunable specificity, stability and oligomerization state has therefore been dramatically facilitated. It has been exploited for various tissue engineering and gene delivery applications,[18] and several proteins including growth factors, transcription factors and antibodies have been grafted onto polymer-based

structures thanks to coiled-coil complexes.[19–22] Our group previously developed two de novo designed peptides, namely the Ecoil and the Kcoil, which design is based on the repetitions of seven distinct amino acids (a heptad). When mixed together, the peptides spontaneously form a coiled-coil heterodimeric complex, which affinity can be modulated by the number of heptads and their sequence, especially the aliphatic residues that comprise the hydrophobic core of the interaction.[23–25] The rationale of this research was to investigate the potential of coiled-coil interactions for the preparation of novel hybrid systems, that is, hydrogels that can deliver biofunctionalized nanoparticles (*e.g.* decorated on their surface with proteins or with encapsulated drugs), at a speed that is not only dependent on particle diffusion or gel degradation but that is tuned by specific affinity interactions.

To produce such system, we developed an Ecoil-decorated nanoparticle that can interact via specific coiled-coil interaction with Kcoil-grafted hydrogel. More precisely, we report, on the one hand, the functionalization of gold nanoparticles (AuNPs) with the Ecoil peptide as well as the human epidermal growth factor (EGF) using a cysteine-tagged Ecoil-EGF chimeric protein. AuNPs are interesting candidates for their biomedical applications in cancer (radiotherapy[26] and photothermal therapy[27]), imaging and drug delivery[28]. Their surface functionalization with therapeutics or peptides is well-documented.[28] On the other hand, we report a polymeric scaffold made from alginate chains that were covalently modified with the complementary Kcoil peptide and designed to specifically interact with decorated AuNPs. Alginate gels indeed feature an excellent biocompatibility, a wide use as injectable gels and unique gelation properties.[29] The AuNPs/hydrogel system was formed by simple coincubation of the Ecoil-bearing nanoparticles with the Kcoil-modified alginate chains during gelation. Affinity-based systems have been reported for protein release from hydrogels, while nanoparticles have been entrapped within gels

for delayed delivery.[5,30] This is however the first report, to the best of our knowledge, that combines both strategies, that is, to sequester nanoparticles within a hydrogel and to release them in a controlled fashion using a specific affinity interaction.[3,31]

The characterization of the biofunctionalized nanoparticles was carried out by dynamic light scattering (DLS), transmission electron microscopy (TEM) and ^{1}H nuclear magnetic resonance (NMR) as well as enzyme-linked immunosorbent assays (ELISA) to assess the bioavailability of both the Ecoil and EGF moieties. The impact of Kcoil concentration in the hydrogel on the diffusive properties of the AuNPs was then investigated using differential dynamic microscopy (DDM) and typical release tests. Both assays indicated that the formation of the Ecoil/Kcoil complex significantly hampered the movement of nanoparticles, and thus that this affinity-based strategy is suitable to prolong the release of NPs from hydrogels. The biological activity of the EGF moiety displayed on the NPs surfaces was also demonstrated by *in vitro* cellular assays, both prior and after their release from the hydrogels.

2. Experimental

2.1 Materials

Cysteine-tagged Ecoil-EGF (CEE) was produced in HEK 293-6E cells and purified by immobilized metal-ion affinity chromatography (IMAC) followed by size-exclusion chromatography, as previously described.[32] Protein concentration was determined by an enzyme-linked immunosorbent assay (ELISA) against EGF and analyzed by SDS-PAGE. Purified CEE was then stored at -80 °C until use. The azidohomoalanine-terminated Kcoil peptides (AhaGG(KVSALKE)$_5$, or Aha-Kcoil) were synthesized by the peptide facility at University of Colorado (Denver, CO). Untagged recombinant human EGF and ELISA kit were purchased from R&D Systems (Minneapolis, MN). Sodium alginate (M_W = 171 kDa) (IL-6G) were purchased from Kimica corporation (New-York, NY). Thiolated polyethylene glycol (PEG-SH) (M_W = 5 kDa) was obtained from Jenkem Technology (Dallas, TX). MilliQ water was generated with a Millipore Gradient A10 purification system. Dulbecco's modified Eagle's medium (DMEM), fetal bovine serum (FBS) and gentamicin were obtained from Gibco (Burlington, VT). 75-cm^2 CellBIND flasks and 48- and 96-well CellBIND plates for cell cultures were purchased from Corning (Corning, NY). All other products and chemicals were purchased from Sigma-Aldrich Canada Ltd. (Oakville, ON), unless otherwise specified. Absorbance measurements were carried out on a Victor V Multilabel Counter from PerkinElmer Inc. (Woodbridge, ON) or using a Spark® multiplate reader from Tecan Group Ltd (Männedorf, Switzerland).

2.2 Biofunctionalization of gold nanoparticles

2.2.1 Synthesis and characterization of gold nanoparticles

Gold nanoparticles (AuNPs) were synthesized using a citrate reduction method according to a previously published procedure.[33] Briefly, trisodium citrate (0.94 mL at 11.4 mg/mL) was rapidly injected in a boiling chloroauric solution (50 mL at 0.1 mg/mL in MQ water) under vigorous stirring and heating for 5 min, then cooled to room temperature (RT). The color of the solution changed from blue to deep red.

The NPs sizes were characterized by dynamic light scattering (DLS) using a Malvern Zetasizer (Malvern, UK) and by transmission electron microscopy (TEM, field emission 2100F, JEOL, Tokyo, Japan). The number of gold atoms per nanoparticle (N) was estimated using [34]

$$N = \frac{\pi \rho D^3}{6\ M}\ , \qquad (1)$$

where ρ is the density for face-centered cubic gold (19.3 g/cm^3), M is the atomic weight of gold (197 g/mol) and D is the diameter of the NPs determined by TEM.

The final AuNPs concentration is given from

$$[AuNPs] = \frac{m}{M \times N \times V}\ , \qquad (2)$$

where m is the initial mass of gold and V is the final volume of the solution. In our experimental conditions, the concentration of the pristine gold nanoparticles was 8.2 10^{11} particles/mL or 1.4 nM, and their diameter was 18 ± 2 nm according to TEM. The stock solution was used to determine the AuNPs extinction coefficient at 531 nm, i.e. ε_{AuNP} = 5.53 10^8 $M^{-1}.cm^{-1}$, which is in good agreement with the literature for particles of this size.[35] After functionalization of the gold nanoparticles, the concentration of coated AuNPs was evaluated via UV-Vis measurements at 531 nm.

2.2.2 PEGylation of gold nanoparticles

After synthesis, the AuNPs were stabilized by means of decoration with a low density of thiolated polyethylene glycol (PEG-SH) (*Mw* = 5 kDa). The gold nanoparticles exposing a low density of PEG (NP-PEG_{LD}) were obtained by injecting ca. 7 µL of PEG-SH in 20 mL of the citrate solution containing the AuNPs (final concentrations of 0.5 µM PEG-SH and 1.4 nM AuNPs). After 16 h under stirring, the NP-PEG_{LD} were centrifuged one time (10,000 × *g* for 30 min) and the supernatant was discarded to remove unreacted PEG-SH.

The amount of PEG-SH on the particles was determined using a ^{1}H NMR-based method as previously described.[36] Briefly, PEGylated NPs (700 µL, 5.4 nM) were digested overnight with 7 µL of Aqua Regia solution (37% HCl and 68-70% HNO_3 in a 3:1 ratio v/v). The resulting mixture was then freeze-dried and resuspended in deuterium oxide (D_2O) to reach a final volume of 700 µL. Acetonitrile (ACN) was used as a standard to quantify the PEG-SH concentrations, i.e. 7 µL of 0.24% v/v ACN in water was added to each sample. The PEG-SH concentration was evaluated by calculating the ratio between the integration of two peaks at specific positions for PEG-SH (3.7 ppm) and ACN (2.06 ppm). The PEG-SH concentration of each sample was determined using a standard curve ranging from 0.1 to 200 µM of PEG-SH.

2.2.3 Cys-Ecoil-EGF grafting on the pegylated gold nanoparticles

The NP-PEG_{LD} were coated with cysteine-tagged Ecoil-EGF (CEE) thanks to the thiol group displayed by the cysteine. NP-PEG_{LD} were mixed with CEE (final concentrations of 1.4 nM and 500 nM, respectively) in MQ water containing dextran chains that acted as a labware non-specific adsorption blocker (10 mg/L of pristine dextran, *Mw* = 70 kDa). The mixture was allowed to react for 16 h under gentle agitation. To enhance NPs stability, PEG-SH was then added at a final concentration of 50 µM for 2 h to generate highly dense PEG-coated NPs (NP-PEG_{HD}). Unreacted

material was removed by performing 4 centrifugations cycles (10,000 × *g* for 30 min). For each cycle, 1.9 mL of supernatant were discarded and the remaining 100 µL of CEE-coated nanoparticles (NP-CEE-PEG_{HD}) were resuspended in 1.9 mL of phosphate buffered saline solution (PBS, 10 mM sodium phosphate and 150 mM of KCl/NaCl salts) supplemented with 0.1% v/v Tween-20 (PBS-T). As controls, NP-PEG_{LD} were incubated with untagged EGF or without added EGF and were subjected to the same purification and blocking procedures. The resulting NPs were named NP-EGF-PEG_{HD} and NP-PEG_{HD}, respectively. The final amount of PEG-SH grafted on NP preparations was determined using the protocol described in the previous section.

2.2.4 EGF quantification

Effectiveness of the CEE grafting on the NPs surface was confirmed by a competitive enzyme-linked immunosorbent assay (ELISA) against EGF. Polystyrene 96-well plates were first saturated with the growth factor overnight (16 h) using 100 µL of 5 nM Ecoil-EGF per well. The wells were then blocked with 50 µL of 1% w/v BSA in PBS for 1 h. In parallel, the NP samples were mixed 1:1 v/v with biotinylated anti-EGF antibodies (100 pM in PBS-T) for 1 h, while known EGF concentrations were mixed with antibodies for calibration. 50 µL of the NPs/antibodies mixtures were then incubated in the EGF pre-coated wells for 1 h. Detection was performed by adding 50 µL of horseradish peroxidase (HRP)-streptavidine conjugate for 20 min followed by a revelation step using 50 µL of substrate solution. A rinsing step was performed after each incubation (3 rinsing cycles with 150 µL of PBS-T). Absorbance was read at 630 nm and 531 nm for correction.

2.3 Bioadhesion of the functionalized nanoparticles

The ability of the Ecoil moiety exposed on the NP-CEE-PEG_{HD} surface to interact with its binding partner, the Kcoil, was assessed by immobilizing functionalized NPs on a Kcoil-coated surface.

Kcoil-bearing dextran surfaces were prepared in 96-well plates as previously described.[22] Functionalized wells were first blocked with BSA (1% w/v in PBS, 100 µL/wells) for 1 h. The NP-CEE-PEG_{HD}, NP-EGF-PEG_{HD} and NP-PEG_{HD} were then injected at a concentration of 140 pM of particles for 1 h. The immobilized NPs were detected using an ELISA against EGF, thanks to a protocol adapted from a previously reported work.[37] Briefly, 50 µL of biotinylated anti-EGF antibodies were added during 30 min. Detection and rinsing steps were carried out as described in the previous section.

2.4 Kcoil grafting on alginate

Kcoil peptides were covalently grafted on alginate via an alkyne-azide click chemistry. Sodium alginate (1.5 g) was first dissolved in 10 mL of 0.5 M NaOH. 6.5 mL of undiluted glycidyl propargyl ether (GPE, 90+% purity) was added and the mixture was allowed to react at RT under agitation for 24 h. The product was then dialyzed (cut-off of 8 kDa) against MQ water for 72 h, freeze-dried and stored at 4 °C until use.

The azide-terminated Kcoil (Aha-Kcoil) was then grafted on the GPE-modified alginate (Alg-GPE). 100 mg of Alg-GPE were dissolved in 10 mL of MQ water with finals concentrations of 1 mM of Tris(3-hydroxypropyltriazolylmethyl)amine (THPTA), 2.5 mM of copper sulfate ($CuSO_4$) and 5 mM of sodium ascorbate. Aha-Kcoil was added at an azide:alkyne ratio of 1:40. The mixture was then allowed to react at RT for 48 h under agitation and in the dark. Note that after 24 h of reaction time, 500 µL of 100 mM sodium ascorbate in MQ water was added in the mixture. Two ultrafiltration cycles in a 100 mM EDTA solution followed by three cycles with MQ water were carried out using Amicon centrifugal filter (cut-off of 5 kDa). The polymer was then freeze-dried and stored at 4 °C until use.

The amount of grafted Kcoil per alginate chain was evaluated by a 2,4,6-Trinitrobenzenesulfonic acid solution (TNBS) assay which allows a quantification of the amines on the peptides. The assay protocol was adapted from previous work.[38,39] Briefly, alginate-Kcoil was diluted at 4 mg/mL in sodium bicarbonate (100 mM, pH 8.5). 100 µL of the solution was mixed with 50 µL of TNBS (0.01% w/v in sodium bicarbonate, 100 mM, pH 8.5) in a 96-well plate. After 2 h at 37°C, 50 µL of sodium dodecyl sulfate (10% w/v in MQ water) and 25 µL of MQ water were added to each well. The absorbance was read at 340 nm and 630 nm for reference. A calibration curve was plotted using known concentration of glycine (range between 4 and 125 µM) and the molar extinction coefficient was corrected by the one for the amine of the lysine side-chain ($\varepsilon_{glycine}$=13400 $M^{-1}.cm^{-1}$ [38] and ε_{lysine}=12000 $M^{-1}.cm^{-1}$).

2.5 NP Release from the alginate matrix

For the NPs release studies, NPs solutions in PBS were mixed with alginate in a 1:1 ratio. More precisely, 8.1 nM of NP-CEE-PEG_{HD} and NP-PEG_{HD} were mixed with solutions containing 80-90% w/w of unmodified alginate plus 10% w/w of GPE-modified, 10% w/w of Kcoil-modified or 20% w/w of Kcoil-modified alginate (resp. Alg-Kcoil0%, Alg-Kcoil10% and Alg-Kcoil20%) for a total of 2% w/v of alginate in water. 50 µL of the mixture (alginate and NPs) were poured in a 96-well plate and gels were formed by adding 50 µL of $CaCl_2$ (0.1 M in water) for 1 h. $CaCl_2$ was then removed and gels were incubated in 200 µL of PBS at RT and under mild agitation (20 RPM). At each timepoint (0, 2, 4, 6, 9, 24 and 72 h), gels were removed from the wells and dissolved with 20 µL of sodium citrate (350 µM). Final volumes were adjusted to 110 µL and the concentration of NPs within the samples was determined by absorbance at 531 nm.

2.6 Differential dynamic microscopy (DDM)

NP-CEE-PEG_{HD} and NP-PEG_{HD} were mixed with Alg-Kcoil10%, Alg-Kcoil20% or MQ water in an equal volume (final concentration of 8.1 nM of nanoparticles and 1% w/v of alginate). 180 µL of the mixtures were injected in 0.4-mm thick glass capillaries (Vitrocom, Canada). Capillaries containing alginate were opened on both ends and incubated in a $CaCl_2$ solution (20 mM) for 24 h for complete gelation to occur. All capillaries were sealed using petroleum jelly prior to DDM experiments.[40] DDM is a correlation-based microscopy technique that enables the characterisation of particle dynamics in complex systems.[41–43] Full details about DDM analysis can be found elsewhere[44–46] and only an overview is presented below.

Videos were recorded at 100 frames per second for 41 seconds using an upright bright-field microscope (Olympus BX81) equipped with a high acquisition-speed camera (Hamamatsu Orca-Flash 4.0 V3) and a 20X magnification phase contrast objective (Olympus Plan Ph1, NA = 0.4). From those movies, power spectrums of the difference between all pairs of images (separated by the same delay time τ) were calculated and averaged yielding the averaged Differential Image Correlation Function $g(\vec{q}, \tau)$. For isotropic motion the azimuthal average was calculated, giving $g(q, \tau) = < g(\vec{q},\tau) >_{\vec{q}}$ with q being the spatial frequency, which under appropriate imaging conditions[44–46] is related to the intermediate scattering function $f(q, \tau)$ probing for particle dynamics so that:

$$g(q,\tau) = A(q)(1 - f(q,t)) + B(q) , \quad (3)$$

where *A(q)* is the amplitude signal and *B(q)* the background noise. Fitting $g(q, \tau)$ with appropriate models of $f(q, \tau)$ can access particle dynamics. We used a generalized exponential:

$$f(q, \tau) = e^{-\left(\frac{\tau}{\tau_R}\right)^{\beta}} \quad (4)$$

where τ_R is the relaxation time and β is an exponent that provides insight about size polydispersity of particles and their interactions. For monodisperse non-interacting spheres in water, $\beta = 1$ and the relaxation time is $\tau_R = \frac{1}{q^2 D}$, with D being the diffusion coefficient from which the particle radius, r, can be extracted following the Stoke-Einstein equation:

$$D = \frac{kT}{6\pi n r} \quad (5)$$

with kT the thermal energy and n the viscosity. $\beta < 1$ usually indicates size polydispersity and/or interactions, be it particle/particle or particle/gel interactions. We found that β was between 0.9 and 1 both in water and in the alginate gels, suggesting that interactions were negligible. We verified that the relaxation times τ_R were proportional to q^{-2}, therefore an effective diffusion coefficient D could be extracted from $\tau_R = q^{-2}D^{-1}$.

2.7 In vitro cell assay

2.7.1 Cell culture

A431 cells overexpressing the EGF receptor were maintained in 75-cm^2 flasks using Dulbecco's modified Eagle's medium (DMEM) supplemented with 10% v/v of fetal bovine serum (FBS) and 0.1% v/v of penicillin-streptomycin. The flasks were kept in a humidified incubator (37 °C, 5% CO_2) until 85-90% confluence.

2.7.2 Phosphorylation assay by Western Blot

A431 cells were distributed in 48-well plates at a concentration of 0.6 10^6 cells/mL (0.5 mL per well). 20 h later, 85-90% of confluence was reached and each well was rinsed 2 times with 1 mL of PBS. Cells were then starved for 3 h using 500 µL of basal medium (DMEM with no serum).

The basal medium was removed from each well and the cells were exposed during 5 min to 50 µL of the functionalized NPs (at an equivalent EGF concentration of 1.5 nM, according to ELISA) or to 50 µL of soluble EGF (EGF concentrations of 0.1, 1 and 10 nM). The wells were washed twice with 1 mL of PBS supplemented with 1 mM of sodium-orthovanadate, and the cells were then lysed using 75 µL of a commercial lysis buffer supplemented with 0.1 mM of sodium-orthovanadate. Insoluble materials were removed by centrifugation (10,000 × *g*, 20 min, 4 °C). Samples were then analysed for phosphotyrosine levels by Western Blot, using mouse PY99 (Santa Cruz, CA) and anti-mouse-HRP antibodies, according to a previously-reported procedure.[47] A Bradford assay was performed prior to gel electrophoresis to ensure that the same amount of protein was loaded in each well. A ChemiDoc system (Biorad, Hercules, CA) and the ImageLab software were used to image the nitrocellulose membrane and to analyse images, respectively. Quantification of the level of phosphorylation in each well was enabled by the *Quantity tools* of the software, using the signal obtained with soluble EGF (10, 1 and 0.1 nM) as a calibration.

3. Results and discussion

We here report the engineering of an affinity-based system for the controlled release of biofunctionalized NPs from a hydrogel, using the high-affinity E/K coiled-coil interactions. This strategy makes use of AuNPs decorated with cysteine-tagged Ecoil-EGF (CEE) and of Kcoil-derivatized alginate hydrogels. AuNPs were stabilized through PEGylation, both before and after CEE functionalization (Figure 1.A), while the Kcoil peptide was grafted on the alginate chains using GPE-mediated alkyne:azide click chemistry (Figure 1.B). We here investigated the diffusive properties of the Ecoil-NPs as a function of Kcoil density in alginate hydrogels (Figure 1.C).

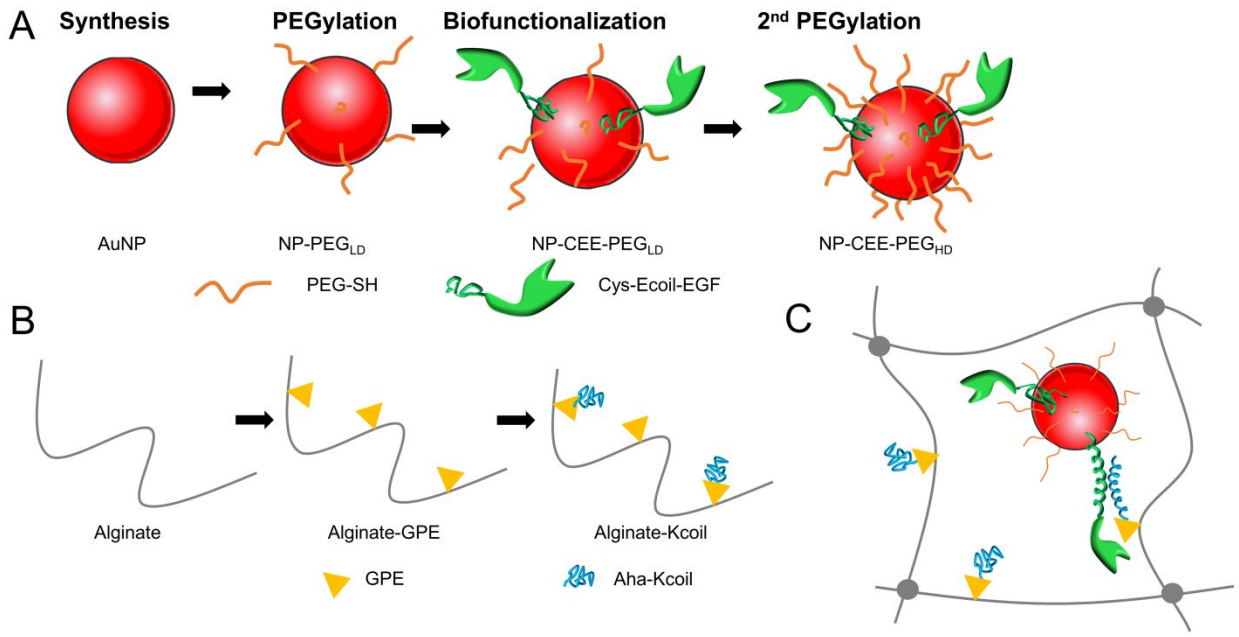

Figure 1. Preparation of the affinity-based hybrid system using gold nanoparticles and an alginate scaffold. (**A**) AuNPs were first PEGylated to a low level for stabilization. Cys-Ecoil-EGF (CEE) was then grafted via thiol-gold chemistry. A second PEGylation step was then performed for higher stability. (**B**) Alginate chains were first derivatized with an alkyne moiety using glycidyl propargyl ether (GPE). Azidohomoalanine-tagged Kcoil peptides (Aha-Kcoil) were then grafted via azide-alkyne click chemistry. (**C**) The dispersion of Ecoil-AuNPs in the Kcoil-alginate hydrogel enabled the formation of the E/K coiled-coil complex to slow down NPs release.

3.1 Characterization of pristine and functionalized NPs

Pristine and functionalized gold nanoparticles (AuNPs) were characterized using transmission electron microscopy (TEM) to determine NPs core diameter, dynamic light scattering (DLS) and differential dynamic microscopy (DDM) for hydrodynamic diameter, ^{1}H nuclear magnetic resonance (NMR) for PEG density, enzyme-linked immunosorbent assays for EGF density and UV-Vis spectroscopy. The data are shown in Table 1 and Figure 2.

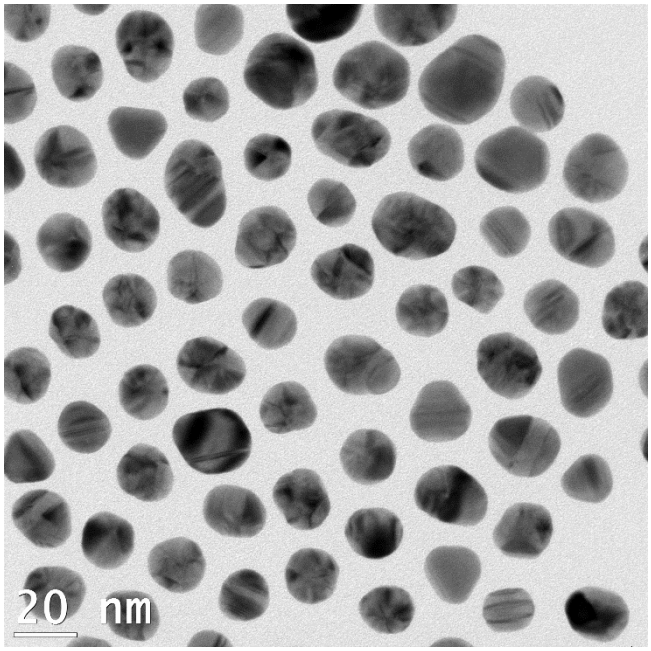

Figure 2 : Transmission electron microscopy (TEM) image of AuNPs.
The average NPs diameter measured was 18 ± 2 nm (n=100).

DLS analysis indicated that the average hydrodynamic diameter of the synthesized AuNPs was $d_{h,DLS} = 28 \pm 0$ nm with a polydispersity index of PDI = 0.29 ± 0.00. Throughout the functionalization process (PEG then CEE then PEG again), the PDI of each NPs type did not significantly change (PDI = 0.29 ± 0.01, 0.31 ± 0.02 and 0.29 ± 0.00 for NP-CEE-PEG_{HD}, NP-EGF-PEG_{HD} and NP-

PEG_{HD} respectively). The hydrodynamic diameter of NP-PEG_{LD} was $d_{h,\ DLS}$ = 55 ± 3 nm, that is, the first PEGylation step induced an increase in diameter of 27 nm, which is in good agreement with the literature.[48] After CEE grafting and a second PEGylation step, the NPs size further increased to reach $d_{h,\ DLS}$ = 62 ± 2 nm. The increase in size (7 nm) between NP-PEG_{LD} and NP-CEE-PEG_{HD} indicated that the first low-density PEG layer allowed for both stabilization and subsequent functionalization. NPs sizes were also determined by DDM. The diffusion coefficient of each type of NPs was first measured in water. NPs sizes were calculated using the Stokes-Einstein equation (Eq. 5) from the measured NPs diffusion coefficient *D*. The sizes of NP-CEE-PEG_{HD} and NP-PEG_{HD} obtained using DDM were close to the values previously determined with DLS (cf. Table 1), while the gap between both techniques can be attributed to a different analysis of the intermediate scattering function (ISF) to take into account polydispersity effects.[44,49] For the NP-PEG_{LD}, the average number of PEG chain per NP was calculated at σ_{PEG} = 0.2 ± 0.1 thousands of PEG chains. Of interest, NP-PEG_{HD} particles had an average number of PEG per NP of σ_{PEG} = 2.6 ± 0.8 whereas NP-CEE-PEG_{HD} and NP-EGF-PEG_{HD} featured dramatically less PEG chains per particle (σ_{PEG} = 0.8 ± 0.3 and σ_{PEG} = 0.5 ± 0.0, respectively), which suggested that the grafting of the protein on the NP surface hampered the grafting of PEG chains during the second PEGylation step.

The impact of the different functionalization on the NPs physical characteristics was also assessed by UV-vis spectroscopy. A significant 4-nm increase in the maximum absorbance wavelength λ_{max} was observed between the NP-PEG_{LD} and the fully functionalized NPs. A competitive ELISA was developed to determine the average number of EGF protein per NP (corresponding to the EGF concentration divided by the NPs concentration). The EGF density, σ_{EGF}, was found to be null (0.0 ± 0.0) for the pegylated NP-PEG_{HD}, whereas σ_{EGF} reached 1.0 ± 0.6 for NP-CEE-PEG_{HD}.

Interestingly, a similar density of σ_{EGF} = 1.2 ± 0.0 protein per particle was also obtained for NPs that were incubated with untagged EGF (NP-EGF-PEG_{HD}). For this sample, the link between untagged EGF and the NP-PEG_{LD} could be attributed to the EGF disulfide bonds interacting with the gold surface, as previously proposed by Song *et al.* [50]

***Table 1** : Characteristics of bare and functionalized gold nanoparticles.*

	AuNP	***NP-PEG$_{LD}$***	***NP-CEE-PEG$_{HD}$***	***NP-EGF-PEG$_{HD}$***	***NP-PEG$_{HD}$***
λ_{max} (nm)[a]	524	524	528	528	528
$d_{h,\ DLS}$ (nm)[b]	28 ± 0	55 ± 3	62 ± 2	64 ± 2	59 ± 2
PDI[c]	0.29 ± 0.00	0.28 ± 0.00	0.29 ± 0.01	0.31 ± 0.02	0.29 ± 0.00
$d_{h,DDM}$ (nm)[d]	-	-	53 ± 2	-	47 ± 0
σ_{PEG} (×10^3)[e]	-	0.2 ± 0.1	0.8 ± 0.3	0.5 ± 0.0	2.6 ± 0.8
σ_{EGF}[f]	-	-	1.0 ± 0.6	1.2 ± 0.0	0.0 ± 0.0

[a] Peak absorbance wavelength

[b] Hydrodynamic diameter determined by DLS (Intensity distribution, mean ± SD, n = 3)

[c] Polydispersity index determined by DLS (Mean ± SD, n = 3)

[d] Hydrodynamic diameter determined by DDM (Mean ± SD, n = 5)

[e] Number of PEG chains per NP (Mean ± SD, n = 3)

[f] Number of EGF per NP (Mean ± SD, n = 3)

3.2 Bioadhesion and bioactivity of the functionalized AuNPs

The ability of the Ecoil moiety present at the NP-CEE-PEG_{HD} surface to interact with its biological partner, the Kcoil peptide, was assessed by incubating the functionalized NPs on Kcoil-decorated multiwell plates. After incubation, the immobilized NP-CEE-PEG_{HD} were detected using an HRP-

labelled anti-EGF antibody. The ELISA data showed a significantly higher signal for NP-CEE-PEG_{HD}, when compared to NP-EGF-PEG_{HD} and NP-PEG_{HD} for which no signal above the noise level was detected (Figure 3.A). The results thus confirmed that a) the Ecoil tag was necessary for NP capture on Kcoil-decorated surfaces and that b) the Ecoil moiety was bioavailable, i.e. both accessible and functional, on the NP-CEE-PEG_{HD}.

As for the EGF moiety on the NP-CEE-PEG_{HD} surface, its biological activity was evaluated by the ability of the growth factor to bind to its cognate receptor (EGFR) and induce EGFR phosphorylation. For that purpose, A431 cells were selected as they are known to express high levels of EGFR.[51] The cells were amplified in DMEM containing 10% v/v FBS until 80-90 % confluence. After a 3 h period of starvation in serum-free medium, the cells were stimulated with either soluble EGF (0 to 10 nM) or functionalized NPs (apparent EGF concentration of 1.5 nM according to ELISA results). The cells were then lysed, cell debris were removed by centrifugation and the amount of phosphorylated EGFR was quantified by Western Blot using an antiphosphotyrosine antibody. The EGFR phosphorylation levels were compared to control soluble EGF at concentrations ranging between 0 to 10 nM. Results show (Figure 3.B) that NP-CEE-PEG_{HD} and NP-EGF-PEG_{HD} were able to induce a higher level of EGFR phosphorylation when compared to soluble EGF. More precisely, when the NP-CEE-PEG_{HD} and NP-EGF-PEG_{HD} particles were diluted to obtain a 1.5 nM concentration of EGF (as determined by ELISA), the phosphorylation levels, that is, the degree of cell stimulation, were close to those obtained with a soluble EGF concentration of 5 ± 2 nM and 13 ± 2 nM, respectively. Of interest, no signal was obtained with NP-PEG_{HD} particles, which confirmed that EGF-free NPs did not induce EGFR phosphorylation. The apparently higher biological activity of the NP-tethered EGF could be the result of the high proximity of the growth factors on the surface of the particles. Indeed, two

proximate EGF are known to promote EGFR dimerization and increase the phosphorylation level compared to their isolated counterparts.[52]

As for the difference between NP-CEE-PEG_{HD} and NP-EGF-PEG_{HD}, it was previously shown that the addition of a Cys-Ecoil N-terminal tag to EGF did not alter the biological activity of the protein in solution.[32] The noticeable difference in EGFR phosphorylation levels obtained with the particles decorated with EGF and CEE could thus be attributed to a higher bioavailability (for instance a better orientation of the EGFR binding site) of EGF on the NP surface, when compared to CEE. The other possible explanation is that the Ecoil, in its random conformation, interacts with EGF binding site decreasing its affinity to its receptor.

Altogether, the phosphorylation assay demonstrated that both cysteine-Ecoil-tagged EGF and untagged EGF grafted on NP-PEG_{LD} were bioactive, and that their immobilization on NP surface did enhance their biological activity. Nonetheless, since our goal is to control the release of NPs via the Ecoil/Kcoil interaction, NP-CEE-PEG_{HD} were selected for further characterization given that NP-EGF-PEG_{HD} could not interact with Kcoil-modified surfaces (cf. Figure 3.A).

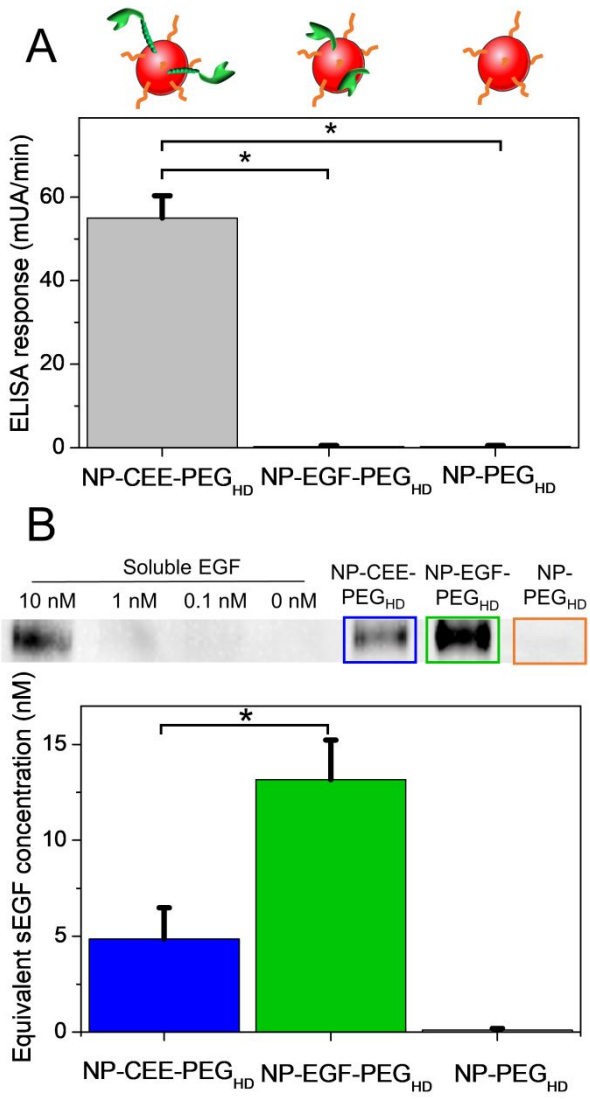

Figure 3. Bioadhesion and bioactivity of functionalized NPs.
(**A**) Bioadhesion on a Kcoil-derivatized surface of NP-CEE-PEG$_{HD}$, NP-EGF-PEG$_{HD}$, and NP-PEG$_{HD}$ as control, as detected by anti-EGF ELISA (n=3) (**B**) EGFR phosphorylation in A431 cells upon binding with soluble EGF (10, 1, 0.1 and 0 nM), NP-CEE-PEG$_{HD}$ or NP-EGF-PEG$_{HD}$ (EGF concentration of 1.5 nM according to ELISA) and NP-PEG$_{HD}$, as monitored by Western Blot. The 180-kDa band immunoreactive to anti-phosphotyrosine antibodies (corresponding to EGFR) was quantified using a ChemiDoc and Image Lab software. Y-axis represents the equivalent concentration in soluble EGF (sEGF) (n = 3 for NP-CEE-PEG$_{HD}$ and NP-EGF-PEG$_{HD}$ and n = 1 for NP-PEG$_{HD}$, * indicates statistical differences between datasets (bilateral t-test, $p < 0.05$).

3.3 Characterization of Kcoil grafting on alginate

Kcoil peptides were grafted on the alginate chains using a two-step method, as illustrated in Figure 4. First, alkyne moieties were conjugated to alginate chain using glycidyl propargyl ether (GPE). L-azidohomoalanine (Aha)-terminated Kcoil was then covalently grafted to the polymer using alkyne-azide click chemistry.[53] In the present experimental conditions, the molar ratio was set to 1 Aha-Koil for 40 alkyne groups.

The alkyne ratio per chain was first quantified by ^{1}H NMR (Figure 4). A peak distinctly appeared at 3.4 ppm (peak A) after the alginate/GPE reaction and was attributed to the proton of the alkyne group. Using the peaks at 5.1 and 5.5 ppm as references (peaks M1 and G1, respectively, that were attributed to protons held by each alginate monomer),[54] we calculated that 29% of the alginate monomers were modified with an alkyne group.

As for the subsequent Kcoil grafting step, the amount of peptide per alginate monomer was evaluated thanks to the TNBS-based amine quantification test. Knowing that 1 Kcoil peptide holds 10 primary amine groups, the TNBS assay revealed that 77 % of the peptides in the alginate-GPE/Aha-Kcoil mixture reacted with alkyne groups. The yield of this click reaction is in good agreement with previous reports that used Aha and alkyne reactive groups.[53,55,56] Altogether, the 171-kDa alginate chains hold an average of 5 Kcoil peptides distributed among the 940 monomers.

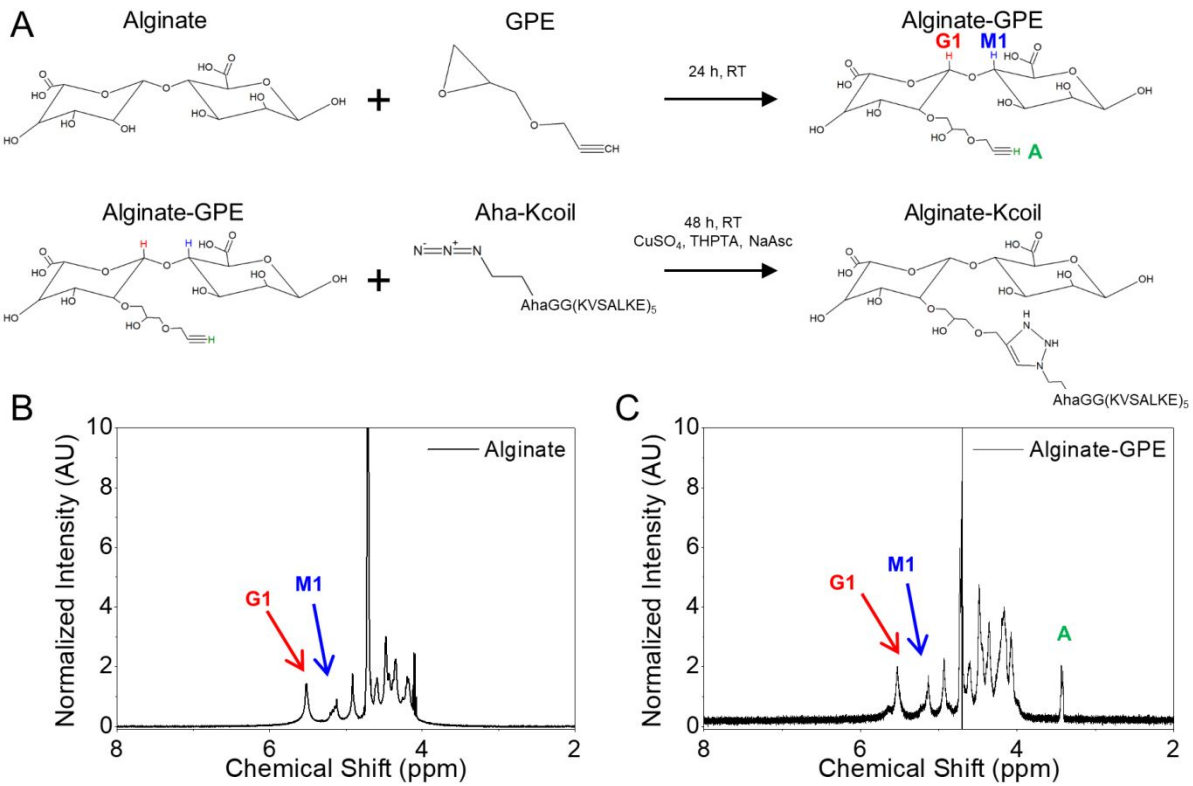

Figure 4. Synthesis and characterization of Kcoil-derivatized alginate.
(**A**) Alginate was first modified with glycidyl propargyl ether (GPE). Azide-terminated Kcoil peptides were then grafted on alginate-GPE via alkyne-azide click chemistry in presence of copper sulfate. (**B** and **C**) The percentage of alkyne-modified monomers was quantified by ^{1}H NMR using the peak at 3.4 ppm (peak A), corresponding to the alkyne, and the peaks at 5.5 ppm (G1) and 5.1 ppm (M1) as reference, corresponding to the total amount of monomers.

3.4 Diffusion and release tests

3.4.1 Diffusion of the functionalized NPs

The diffusion of functionalized and pegylated NPs in alginate gels was investigated by DDM. Solutions of 2% w/v alginate containing either 10% or 20% w/w of Kcoil-modified alginate were mixed in a 1:1 (v/v) ratio with 16.3 pM of either NP-CEE-PEG_{HD} or NP-PEG_{HD}. The mixtures were injected in capillaries opened on both ends and were then immersed in a solution of 20 mM $CaCl_2$, which initiated the gelation by diffusion of Ca^{2+} ions. After 24 h, videos were taken at 100

fps for 41 s and the results are shown in Figure 5. Intermediate scattering functions (ISFs) *f(q,τ)* were extracted from the autocorrelation function as described above. In the case of Alg-Kcoil10%, a second slower dynamic process was observed, that was presumably due to a slow gel drift or the presence of a few aggregates as observed from the recorded videos. For such cases, we used a double generalised exponential model (from equations 3 and 4) for the ISFs when fitting the DICF g*(q,τ)*:

$$g(q,\tau) = A_1(q)(1 - f_1(q,\tau)) + A_2(q)(1 - f_2(q,\tau)) + B(q) \quad (6)$$

where indices 1 and 2 respectively correspond to the short-time (NPs contribution) and long-time (aggregate/drift contribution) processes. We only considered the short-time diffusion coefficients in what follows.

In Figure 5.A, we express the evolution of the ISF *f(q,τ)* as a function of the relaxation time τ_R rescaled with the spatial frequency q^2 to give insight of the dynamic process. This rescaling makes the ISFs quantitatively comparable over variable *q*-ranges for all media considered, when considering diffusive process with $D = q^{-2} \tau_R^{-1}$. These functions show the same dynamic processes for NP-CEE-PEG_{HD} and NP-PEG_{HD} that decorrelate at $\tau_R q^2 \sim 0.11$ s/μm^2 (D ~ 8-9 μm^2/s) in water and at $\tau_R q^2 \sim 0.71$ s/μm^2 (D ~ 1.3-1.5 μm^2/s) in Alg-Kcoil10%. However, in Alg-Kcoil20%, ISFs corresponding to NP-CEE-PEG_{HD} or NP-PEG_{HD} do not overlap, indicating different diffusion coefficient. In all cases, the stretching exponent, β, was found between 0.9 and 1, which implies that no significant interaction between the NPs and the gels were observed in DDM.

From ISFs, τ_R values were extracted to determine the diffusion coefficient of the NPs in both Alg-Kcoil10% and Alg-Kcoil20% gels. Diffusion coefficients *D* were found independent of *q*, suggesting a diffusive motion within alginate gels as depicted in insets of Figure 5.A. The ratios

between diffusion coefficients of NPs measured in the gels, D, and in water, D_w, are presented in Figure 5.B.

In Alg-Kcoil10%, no difference in D/D_w was observed between NP-CEE-PEG_{HD} and NP-PEG_{HD}: both diffusion coefficients decreased to *ca.* 14% of the value that was obtained in water. Interestingly, for NP-PEG_{HD}, the D/D_w ratio increased from 0.15 ± 0.01 in Alg-Kcoil10% to 0.39 ± 0.07 in Alg-Kcoil20%. This could be due to differences in the structural properties of the hydrogels. Indeed, Alg-Kcoil20% has a higher concentration of unreacted hydrophobic alkyne and amphipathic Kcoil moieties than Alg-Kcoil10%.

A significant difference between particles was nonetheless observed in Alg-Kcoil20%, where the D/D_w of NP-CEE-PEG_{HD} was found to be significantly lower than NP-PEG_{HD} (D/D_w of 0.25 ± 0.01 and 0.39 ± 0.07, respectively). This observation demonstrates that NP-CEE-PEG_{HD} were slowed down by a factor of 4 in Alg-Kcoil20% when compared to water, as opposed to a factor of *ca.* 2.6 for NP-PEG_{HD}. The data thus demonstrated that the specific interaction between Kcoil (with sufficient concentration) and Cys-Ecoil-EGF had a significant impact on the diffusive properties of nanoparticles.

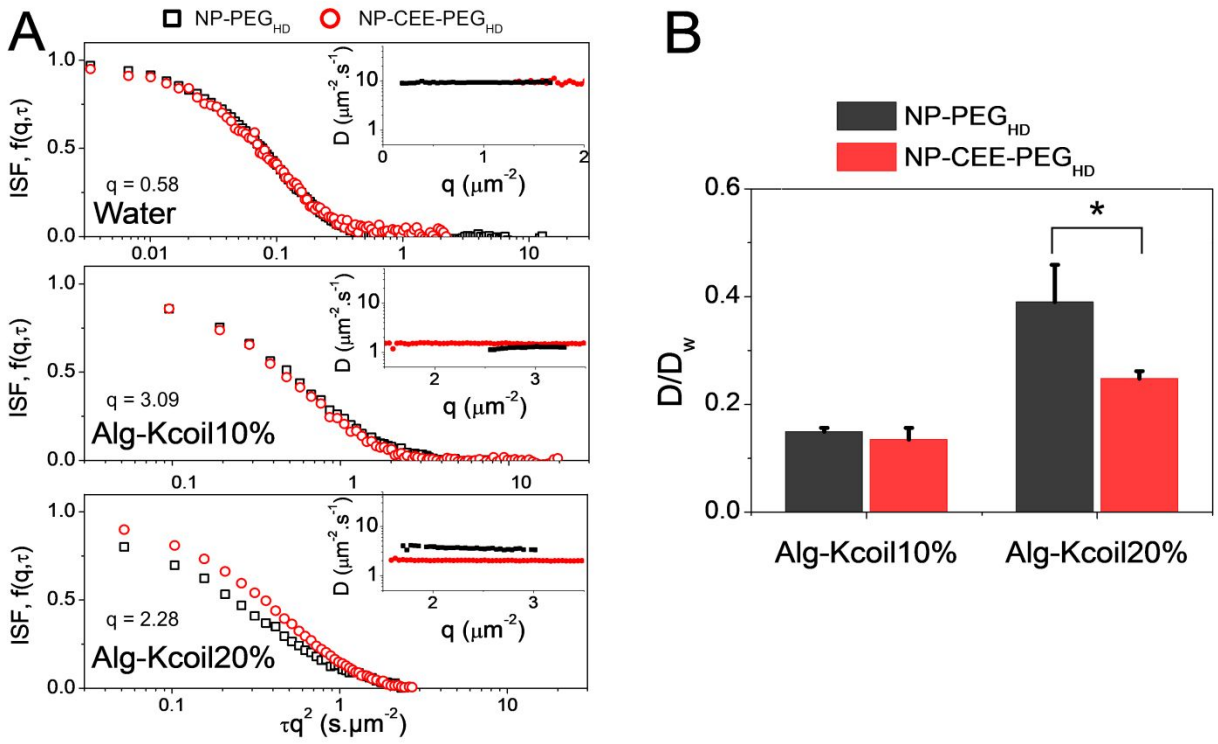

Figure 5. Diffusive properties of NPs assessed by differential dynamic microscopy. (**A**) Intermediate scattering function $f(q,\tau)=\exp(-(\tau/\tau_R)^{\beta})$ of NP-CEE-PEG$_{HD}$ (red circles) and NP-PEG$_{HD}$ (black squares) in water, Alg-Kcoil10% and Alg-Kcoil20%. In Alg-Kcoil10%, ISF were calculated using a double exponential as in Eq.6. Insets represent the coefficient diffusion D (averaged from 5 videos) vs q for each type of NPs. Different q-values were used for each medium to best represent the short-time plateau and the long-time plateau of the ISF. (**B**) Diffusion coefficients of NP-CEE-PEG$_{HD}$ and NP-PEG$_{HD}$, as determined by DDM. The Y-axis represents the ratio between the coefficients of diffusion of NPs in the hydrogels, D, and in water, D_w. * indicates statistical differences between datasets (n = 5) (bilateral t-test, $p < 0.05$).

3.4.2 NPs release from biofunctionalized hydrogels

The diffusive properties of the particles in hydrogels were further investigated in release studies. NP-CEE-PEG$_{HD}$ and NP-PEG$_{HD}$ particles were added to a 1% (total w/v) alginate solution containing 80-90% (w/v) of unmodified alginate supplemented with 10% of Alg-GPE, 10% of Alg-Kcoil or 20% of Alg-Kcoil, respectively referred to as Alg-Kcoil0%, Alg-Kcoil10% and Alg-

Kcoil20%. The solutions were poured in multiwell plates and gelled by the addition of $CaCl_2$ for 1 h. After gel formation, each gel was incubated in PBS. The concentration of AuNPs that were released in the incubation medium was indirectly assessed at different timepoints by measuring the number of NPs still entrapped in the hydrogels (Figure 6).

As a starting point, we observed the release profiles of NP-PEG_{HD} in different alginate medium. We found that their release was slightly affected by the gel composition, where the higher the Kcoil concentration was (from 0% to 10% and to 20%), the faster the NP-PEG_{HD} particles were released. This increase in release rate was observed since the first day, with respectively 68.4, 78.7 and 86.0% of NP-PEG_{HD} released after 24 h, in qualitative agreement with the DDM results (Figure 5). As mentioned, we ascribe this difference by the presence of Kcoil and/or the unreacted alkyne moieties altering the structural properties (porosity) of the gel. Indeed, chains pending from the alginate skeleton can affect crosslinking by preventing the alignment of the alginate chains and thus the formation of the so-called "egg box" structure by which alginate crosslinks with calcium cations.[57] The mechanical properties of the hydrogels were thus investigated using an indentation assay. A decreasing trend between Alg-Kcoil0%, Alg-Kcoil10% and Alg-Kcoil20% was observed, with Young's modulus values of 360, 215 and 137, respectively. The data thus suggested that mechanical cohesion of the gel decreased with an increasing amount of GPE content (see Supplementary Information, Figure S1).

For NP-CEE-PEG_{HD}, the general trend observed in the release profile studies was opposite to the one obtained with NPs that bore PEG moieties only. Indeed, there was no increase of NP-CEE-PEG_{HD} release from Alg-Kcoil0% to Alg-Kcoil20% during the first 9 h. Moreover, after 24 h on, the fraction of NP-CEE-PEG_{HD} that was retained inside the gels was significantly higher in the Alg-Kcoil20% hydrogel than in hydrogels with lower Kcoil content. More precisely, 42 ± 3 % of

the NP-CEE-PEG_{HD} diffused out of the Alg-Kcoil20% hydrogel to the surrounding PBS medium after 24 h, while 63 ± 4 % and 62 ± 8 % of the particles were released from Alg-Kcoil10% and Alg-Kcoil0%, respectively (Figure 5). In Alg-Kcoil20% at 24 h, Ecoil-decorated nanoparticles, NP-CEE-PEG_{HD}, were retained twice as much as the nanoparticles with PEG only (42% and 86% of release, respectively). Interestingly, there were no statistically significant differences between NP-CEE-PEG_{HD} and NP-PEG_{HD} in Alg-Kcoil0% at any timepoint ($n \geq 4$, $p > 0.05$). This showed that (a) the surface presentation of Cys-Ecoil-EGF had no detectable influence on NPs release in absence of Kcoil and that (b) differences in NPs surface chemistry did not affect the structure of the gel. The variations in release fraction between NP-PEG_{HD} and NP-CEE-PEG_{HD} in the Kcoil-containing hydrogels could therefore not be attributed to CEE/alginate interactions but rather confirmed that the surface presentation of the Ecoil-tagged protein hindered the mobility and decreased the release of nanoparticles via the formation of the Ecoil/Kcoil complex.

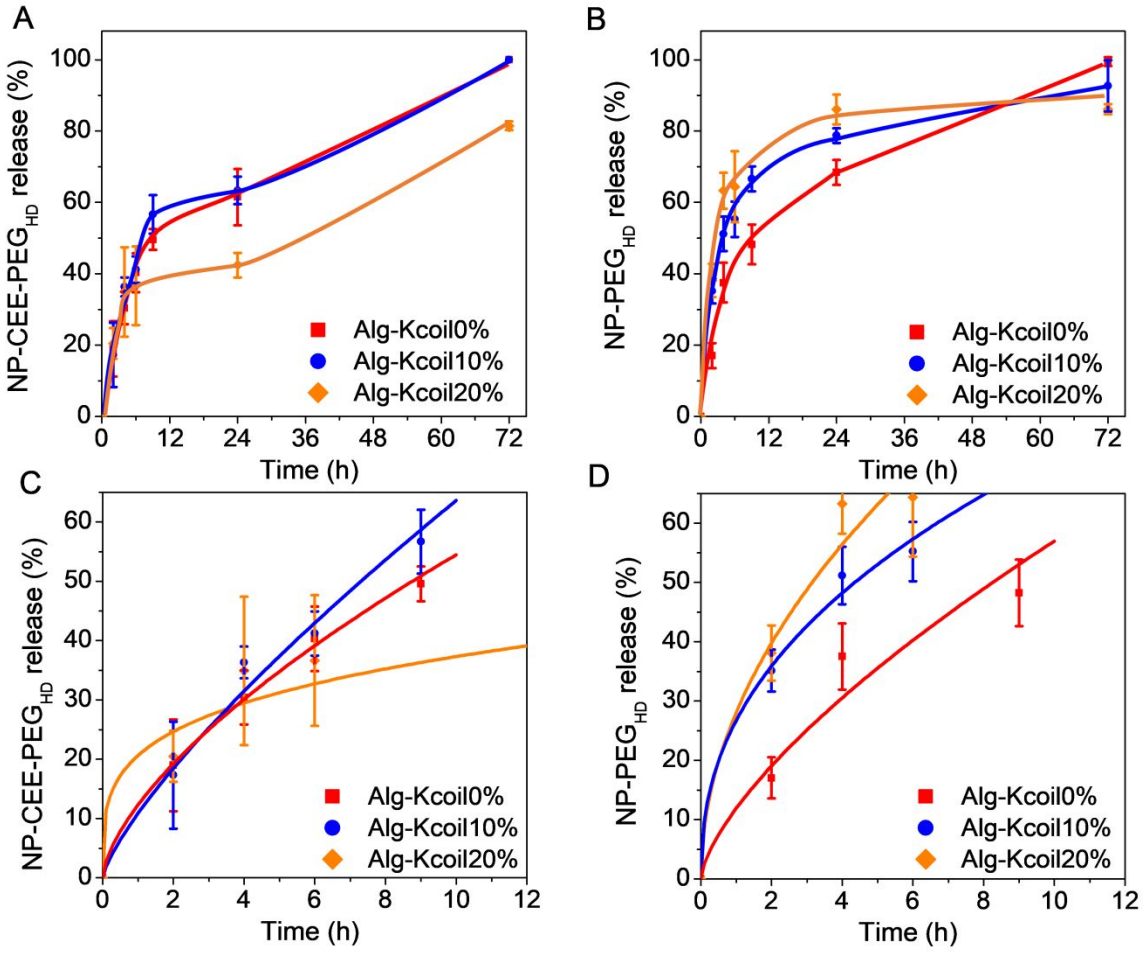

Figure 6. NPs release from Kcoil-modified alginate hydrogels. NP-CEE-PEG$_{HD}$ (A) and NP-PEG$_{HD}$ (B) are released from Alg-Kcoil0%, Alg-Kcoil10% and Alg-Kcoil20%, as calculated from the number of NPs still entrapped in the gel relative to t = 0. NP-CEE-PEG$_{HD}$ (C) and NP-PEG$_{HD}$ (D) data were fitted with a power-law model: each exponent was found to be between 0.43 and 1, characteristic of diffusion (both Fickian and non-Fickian), except for NP-CEE-PEG$_{HD}$ in Alg-Kcoil20%. (n≥4)

Altogether, the data revealed that the introduction of the Kcoil peptide in the hydrogel and its Ecoil partner on the nanoparticles slowed down the release of particles thanks to specific Ecoil/Kcoil interactions, despite conflicting changes in the bulk properties of the gel. So to understand the mechanism behind NP release, the experimental NPs release curves were fitted using a power-law model as described by Ritger and Peppas:[58,59]

$$y = kt^n \,, \qquad (6)$$

where y is the fractional solute release, k is a constant, t the release time and n is the diffusional exponent. The fitted parameters are shown in Table 2.

In all but one case, diffusional exponents were found between 0.43 and 1, which is characteristic of a purely diffusive mechanism (0.43 being purely Fickian and]0.43;1[describing an anomalous transport, i.e. a mix of Fickian and non-Fickian diffusions). For NP-CEE- PEG_{HD} in Alg-Kcoil20% only, a diffusional exponent n of 0.25 was calculated, which means that the power-law model cannot be applied and that the release mechanism cannot be explained by diffusion only. In that specific case, it was thus apparent that another mechanism was contributing to the release of the particles, most likely the specific Ecoil/Kcoil interaction.

It is also worth mentioning that the initial burst release of NP-CEE-PEG_{HD} was both larger and longer in Alg-Kcoil10% (ca. 60% of total NPs between 0 and 9 h) than in Alg-Kcoil20% (ca. 40% of total NPs within 6 h, Figure 5.A). Following this burst, the behavior of the particles in all three gels was highly similar: little to no particle release from 12 to 24 h, then a slow and steady release with the same apparent rate between 24 and 72 h (36 to 39% of particle loss). The release rates measured after 24 h could be explained by gel erosion (which was noticed when manipulating the gels). Indeed, nanoparticles could be released along with the alginate chains whether they contained Kcoil moieties or not. This would have also occurred in hydrogels containing NP-PEG_{HD}, even though it would have been difficult to observe given that the amount released at 24 h was already very high (ca. 85%). When comparing NP-CEE-PEG_{HD} with NP-PEG_{HD} in Alg-Kcoil20%, the release mechanism thus appeared as two-fold: first, a slow release of particles

decorated with Ecoil moieties only, thanks to Ecoil/Kcoil interactions, and second, gel erosion that caused the release of NP-CEE-PEG_{HD} to catch up with the release of NP-PEG_{HD}.

Table 2: Results of the fitting parameters obtained using Eq. 6

	NP-CEE-PEG$_{HD}$			***NP-PEG$_{HD}$***		
	n	k	R^2	n	k	R^2
Alg-Kcoil0%	0.65	0.12	1.00	0.68	0.12	0.89
Alg-Kcoil10%	0.77	0.11	0.96	0.43	0.27	0.95
Alg-Kcoil20%	0.26	0.21	0.72	0.50	0.28	0.89

n: exponent of the power-law, included between 0.43 and 1 for the model

k: multiplication factor of the Power Law

R^2: determination coefficient of the fittings

Parameters were fitted using a linear regression on ln(y) = f(ln(t))

Altogether, both DDM and release tests demonstrated that coiled-coil interactions have a significant impact on the diffusive properties of the nanoparticles in hydrogels by slowing their release, from the combination of the structure of the gel and coil interactions. DDM was found to be a useful predictor of the release flux of NPs in gels by characterizing their diffusion coefficient *D* and correlating it to actual release of NPs.

3.4.3 Bioactivity of released NPs

To assess the biological potency of the NPs that were first entrapped in gels then released in PBS (for a total of 72 h spent in the multiwell plate), an EGFR phosphorylation assay was conducted as previously described. The NP-CEE-PEG_{HD} that were collected after their release showed a

strong phosphorylation induction, to an extent highly similar to fresh NPs and equivalent to 4.4 nM of soluble EGF (to be compared with 4.9 nM for fresh particles, cf. Figure 3).This experiment highlighted that the bioactivity of the EGF moiety on the surface of the released NP remained unaffected by the trapping and release process, critical to achieve any desired therapeutic response. This further strengthened our confidence in coiled-coil affinity-based drug delivery system as versatile tool to deliver, in a timely manner, nanoparticles to a specific tissue, as here explored for cells expressing EGF receptors.

4. Conclusions

Herein we report the use of coiled-coil interactions to extend the release rate of EGF-decorated gold nanoparticles from an alginate hydrogel. The proposed approach relies on the covalent grafting of the Ecoil peptide on NPs and its complementary partner, the Kcoil, on alginate chains. As a proof of concept, we showed that, when compared to AuNPs with PEG only, AuNPs decorated with both the Ecoil peptide and the epidermal growth factor were released more slowly from hydrogels that featured a high Kcoil peptide content. The released AuNPs were still able to induce EGFR-receptor activation via surface-grafted EGF.

To the best of our knowledge, we here showed for the first time that the delivery of a bioactive cue can be controlled by using an affinity-based hybrid system, that is, a nanoparticular carrier entrapped within a hydrogel using specific affinity interactions. This strategy offers a wide range of applications. Gold NPs have indeed been widely used in photothermal therapy, radiotherapy, imaging and drug delivery. This system could also be applied to other types of nanoparticles (e.g.

liposomes or polymeric NPs) for the delivery of either hydrophilic or hydrophobic drugs. Indeed, the use of coiled-coil peptides provides a high level of versatility, as these peptides are highly stable and can be grafted on virtually any molecule or structure. Moreover, the rationale design of the peptide sequences should allow for a high level of tunability in the thermodynamics of the interaction and therefore in the release rates of the therapeutics of interest.

ASSOCIATED CONTENT

Supporting Information: Mechanical properties of alginate hydrogels (indentation assays) and estimation of pore size.

AUTHOR INFORMATION

Corresponding Authors

*E-mail: gregory.decrescenzo@polymtl.ca.

*E-mail: xavier.banquy@umontreal.ca.

AUTHOR CONTRIBUTIONS

The manuscript was written through contributions of all authors.

ORCID

Xavier Banquy: 0000-0002-3342-3179

Gregory De Crescenzo: 0000-0002-6280-1570

Frederic Murschel: 0000-0002-6735-8934

CONFLICTS OF INTEREST

The authors declare no competing financial interest.

ACKNOWLEDGMENT

This work was supported by the Canada Research Chairs on Protein-enhanced Biomaterials (G.D.C.) and on Bioinspired Materials (X.B.), by the Natural Sciences and Engineering Research Council of Canada Discovery Grant (P.L.L., G.D.C. and X.B.), by the Biomedical Science and Technology Research Group (B.L., F.M., and G.D.C.) and the Fonds de Recherche du Québec – Nature et Technologies (F.M.). V.A.M. acknowledges financial support from a ERC-2013-AdG 340877-PHYSAPS. The present work was funded by the TransMedTech Institute (B.L. and F.M.) and its main funding partner, the Canada First Research Excellence Fund. We would like to thank S. Bilodeau for NMR measurements and C. Ribeiro for ELISA assay.

REFERENCES

(1) El-Say, K. M.; El-Sawy, H. S. Polymeric Nanoparticles: Promising Platform for Drug Delivery. *Int. J. Pharmaceut.* **2017**, *528* (1), 675–691. https://doi.org/10.1016/j.ijpharm.2017.06.052.

(2) Hassan, S.; Prakash, G.; Bal Ozturk, A.; Saghazadeh, S.; Farhan Sohail, M.; Seo, J.; Remzi Dokmeci, M.; Zhang, Y. S.; Khademhosseini, A. Evolution and Clinical Translation of Drug Delivery Nanomaterials. *Nano Today* **2017**, *15*, 91–106. https://doi.org/10.1016/j.nantod.2017.06.008.

(3) Vulic, K.; Shoichet, M. S. Affinity-Based Drug Delivery Systems for Tissue Repair and Regeneration. *Biomacromolecules* **2014**, *15* (11), 3867–3880. https://doi.org/10.1021/bm501084u.

(4) Kakkar, A.; Traverso, G.; Farokhzad, O. C.; Weissleder, R.; Langer, R. Evolution of Macromolecular Complexity in Drug Delivery Systems. *Nat. Rev. Chem.* **2017**, *1* (8), 0063. https://doi.org/10.1038/s41570-017-0063.

(5) Delplace, V.; Obermeyer, J.; Shoichet, M. S. Local Affinity Release. *ACS Nano* **2016**, *10* (7), 6433–6436. https://doi.org/10.1021/acsnano.6b04308.

(6) Freeman, I.; Cohen, S. The Influence of the Sequential Delivery of Angiogenic Factors from Affinity-Binding Alginate Scaffolds on Vascularization. *Biomaterials* **2009**, *30* (11), 2122–2131. https://doi.org/10.1016/j.biomaterials.2008.12.057.

(7) Lin, C.-C.; Anseth, K. S. Controlling Affinity Binding with Peptide-Functionalized Poly(Ethylene Glycol) Hydrogels. *Adv. Funct. Mater.* **2009**, *19* (14), 2325. https://doi.org/10.1002/adfm.200900107.

(8) Battig, M. R.; Soontornworajit, B.; Wang, Y. Programmable Release of Multiple Protein Drugs from Aptamer-Functionalized Hydrogels via Nucleic Acid Hybridization. *J. Am. Chem. Soc.* **2012**, *134* (30), 12410–12413. https://doi.org/10.1021/ja305238a.

(9) Mulyasasmita, W.; Cai, L.; Hori, Y.; Heilshorn, S. C. Avidity-Controlled Delivery of Angiogenic Peptides from Injectable Molecular-Recognition Hydrogels. *Tissue Eng. Part A* **2014**, *20* (15–16), 2102–2114. https://doi.org/10.1089/ten.tea.2013.0357.

(10) Thatiparti, T. R.; Shoffstall, A. J.; von Recum, H. A. Cyclodextrin-Based Device Coatings for Affinity-Based Release of Antibiotics. *Biomaterials* **2010**, *31* (8), 2335–2347. https://doi.org/10.1016/j.biomaterials.2009.11.087.

(11) J. Webber, M.; Langer, R. Drug Delivery by Supramolecular Design. *Chem. Soc. Rev.* **2017**, *46* (21), 6600–6620. https://doi.org/10.1039/C7CS00391A.

(12) Cheng, H.; Chawla, A.; Yang, Y.; Li, Y.; Zhang, J.; Jang, H. L.; Khademhosseini, A. Development of Nanomaterials for Bone-Targeted Drug Delivery. *Drug Disc. Today* **2017**, *22* (9), 1336–1350. https://doi.org/10.1016/j.drudis.2017.04.021.

(13) Vermonden, T.; Censi, R.; Hennink, W. E. Hydrogels for Protein Delivery. *Chem. Rev.* **2012**, *112* (5), 2853–2888. https://doi.org/10.1021/cr200157d.

(14) Rambhia, K. J.; Ma, P. X. Controlled Drug Release for Tissue Engineering. *J. Controlled Release* **2015**, *219*, 119–128. https://doi.org/10.1016/j.jconrel.2015.08.049.

(15) Parry, D. A. D.; Fraser, R. D. B.; Squire, J. M. Fifty Years of Coiled-Coils and Alpha-Helical Bundles: A Close Relationship between Sequence and Structure. *J. Struct. Biol.* **2008**, *163* (3), 258–269. https://doi.org/10.1016/j.jsb.2008.01.016.

(16) Apostolovic, B.; Danial, M.; Klok, H.-A. Coiled Coils: Attractive Protein Folding Motifs for the Fabrication of Self-Assembled, Responsive and Bioactive Materials. *Chem. Soc. Rev.* **2010**, *39* (9), 3541–3575. https://doi.org/10.1039/b914339b.

(17) Eskandari, S.; Guerin, T.; Toth, I.; Stephenson, R. J. Recent Advances in Self-Assembled Peptides: Implications for Targeted Drug Delivery and Vaccine Engineering. *Adv. Drug Deliv. Rev.* **2017**, *110–111*, 169–187. https://doi.org/10.1016/j.addr.2016.06.013.

(18) Wu, Y.; Collier, J. H. α-Helical Coiled-Coil Peptide Materials for Biomedical Applications. *Wiley Interdiscip. Rev. Nanomed. Nanobiotechnol.* **2017**, *9* (2), e1424. https://doi.org/10.1002/wnan.1424.

(19) Pechar, M.; Pola, R.; Laga, R.; Ulbrich, K.; Bednárová, L.; Maloň, P.; Sieglová, I.; Král, V.; Fábry, M.; Vaněk, O. Coiled Coil Peptides as Universal Linkers for the Attachment of Recombinant Proteins to Polymer Therapeutics. *Biomacromolecules* **2011**, *12* (10), 3645–3655. https://doi.org/10.1021/bm200897b.

(20) Assal, Y.; Mizuguchi, Y.; Mie, M.; Kobatake, E. Growth Factor Tethering to Protein Nanoparticles via Coiled-Coil Formation for Targeted Drug Delivery. *Bioconjugate Chem.* **2015**, *26* (8), 1672–1677. https://doi.org/10.1021/acs.bioconjchem.5b00266.

(21) Siew, S.; Kaneko, M.; Mie, M.; Kobatake, E. Construction of a Tissue-Specific Transcription Factor-Tethered Extracellular Matrix Protein via Coiled-Coil Helix Formation. *J. Mater. Chem. B* **2016**, *4* (14), 2512–2518. https://doi.org/10.1039/C5TB01579K.

(22) Noel, S.; Fortier, C.; Murschel, F.; Belzil, A.; Gaudet, G.; Jolicoeur, M.; De Crescenzo, G. Co-Immobilization of Adhesive Peptides and VEGF within a Dextran-Based Coating for Vascular Applications. *Acta Biomater.* **2016**, *37*, 69–82. https://doi.org/10.1016/j.actbio.2016.03.043.

(23) De Crescenzo, G.; Litowski, J. R.; Hodges, R. S.; O'Connor-McCourt, M. D. Real-Time Monitoring of the Interactions of Two-Stranded de Novo Designed Coiled-Coils: Effect of Chain Length on the Kinetic and Thermodynamic Constants of Binding. *Biochemistry* **2003**, *42* (6), 1754–1763. https://doi.org/10.1021/bi0268450.

(24) Murschel, F.; Fortier, C.; Jolicoeur, M.; Hodges, R. S.; De Crescenzo, G. Two Complementary Approaches for the Controlled Release of Biomolecules Immobilized via Coiled-Coil Interactions: Peptide Core Mutations and Multivalent Presentation. *Biomacromolecules* **2017**, *18* (3), 965–975. https://doi.org/10.1021/acs.biomac.6b01830.

(25) Litowski, J. R.; Hodges, R. S. Designing Heterodimeric Two-Stranded α-Helical Coiled-Coils: The Effect of Chain Length on Protein Folding, Stability and Specificity. *The Journal of Peptide Research* **2001**, *58* (6), 477–492. https://doi.org/10.1034/j.1399-3011.2001.10972.x.

(26) Her, S.; Jaffray, D. A.; Allen, C. Gold Nanoparticles for Applications in Cancer Radiotherapy: Mechanisms and Recent Advancements. *Adv. Drug Deliv. Rev.* **2017**, *109*, 84–101. https://doi.org/10.1016/j.addr.2015.12.012.

(27) Riley, R. S.; Day, E. S. Gold Nanoparticle-Mediated Photothermal Therapy: Applications and Opportunities for Multimodal Cancer Treatment. *Wiley Interdiscip. Rev. Nanomed. Nanobiotechnol.* **2017**, *9* (4), e1449. https://doi.org/10.1002/wnan.1449.

(28) Kong, F.-Y.; Zhang, J.-W.; Li, R.-F.; Wang, Z.-X.; Wang, W.-J.; Wang, W. Unique Roles of Gold Nanoparticles in Drug Delivery, Targeting and Imaging Applications. *Molecules* **2017**, *22* (9), 1445. https://doi.org/10.3390/molecules22091445.

(29) Agüero, L.; Zaldivar-Silva, D.; Peña, L.; Dias, M. L. Alginate Microparticles as Oral Colon Drug Delivery Device: A Review. *Carbohydr. Polym.* **2017**, *168*, 32–43. https://doi.org/10.1016/j.carbpol.2017.03.033.

(30) Zhao, F.; Yao, D.; Guo, R.; Deng, L.; Dong, A.; Zhang, J. Composites of Polymer Hydrogels and Nanoparticulate Systems for Biomedical and Pharmaceutical Applications. *Nanomaterials (Basel)* **2015**, *5* (4), 2054–2130. https://doi.org/10.3390/nano5042054.

(31) Mauri, E.; Papa, S.; Masi, M.; Veglianese, P.; Rossi, F. Novel Functionalization Strategies to Improve Drug Delivery from Polymers. *Expert Opin. Drug Deliv.* **2017**, *14* (11), 1305–1313. https://doi.org/10.1080/17425247.2017.1285280.

(32) Riahi, N.; Murschel, F.; Lerouge, S.; Durocher, Y.; Henry, O.; De Crescenzo, G. Bioavailability of Immobilized Epidermal Growth Factor: Covalent versus Noncovalent Grafting. *Biointerphases* **2017**, *12* (1), 010501. https://doi.org/10.1116/1.4978871.

(33) Kumar, S.; Aaron, J.; Sokolov, K. Directional Conjugation of Antibodies to Nanoparticles for Synthesis of Multiplexed Optical Contrast Agents with Both Delivery and Targeting Moieties. *Nature Protocols* **2008**, *3* (2), 314–320. https://doi.org/10.1038/nprot.2008.1.

(34) Hinterwirth, H.; Kappel, S.; Waitz, T.; Prohaska, T.; Lindner, W.; Lämmerhofer, M. Quantifying Thiol Ligand Density of Self-Assembled Monolayers on Gold Nanoparticles by Inductively Coupled Plasma–Mass Spectrometry. *ACS Nano* **2013**, *7* (2), 1129–1136. https://doi.org/10.1021/nn306024a.

(35) Liu, X.; Atwater, M.; Wang, J.; Huo, Q. Extinction Coefficient of Gold Nanoparticles with Different Sizes and Different Capping Ligands. *Colloids Surf. B Biointerfaces* **2007**, *58* (1), 3–7. https://doi.org/10.1016/j.colsurfb.2006.08.005.

(36) Smith, A. M.; Marbella, L. E.; Johnston, K. A.; Hartmann, M. J.; Crawford, S. E.; Kozycz, L. M.; Seferos, D. S.; Millstone, J. E. Quantitative Analysis of Thiolated Ligand Exchange on Gold Nanoparticles Monitored by 1H NMR Spectroscopy. *Anal. Chem.* **2015**, *87* (5), 2771–2778. https://doi.org/10.1021/ac504081k.

(37) Murschel, F.; Liberelle, B.; St-Laurent, G.; Jolicoeur, M.; Durocher, Y.; De Crescenzo, G. Coiled-Coil-Mediated Grafting of Bioactive Vascular Endothelial Growth Factor. *Acta Biomaterialia* **2013**, *9* (6), 6806–6813. https://doi.org/10.1016/j.actbio.2013.02.032.

(38) Spellman, D.; McEvoy, E.; O'Cuinn, G.; FitzGerald, R. J. Proteinase and Exopeptidase Hydrolysis of Whey Protein: Comparison of the TNBS, OPA and PH Stat Methods for Quantification of Degree of Hydrolysis. *International Dairy Journal*. 13th ed. 2003, pp 447–453.

(39) Noel, S.; Liberelle, B.; Robitaille, L.; De Crescenzo, G. Quantification of Primary Amine Groups Available for Subsequent Biofunctionalization of Polymer Surfaces. *Bioconjug. Chem.* **2011**, *22* (8), 1690–1699. https://doi.org/10.1021/bc200259c.

(40) Cerbino, R.; Trappe, V. Differential Dynamic Microscopy: Probing Wave Vector Dependent Dynamics with a Microscope. *Phys. Rev. Lett.* **2008**, *100* (18), 188102. https://doi.org/10.1103/PhysRevLett.100.188102.

(41) Edera, P.; Bergamini, D.; Trappe, V.; Giavazzi, F.; Cerbino, R. Differential Dynamic Microscopy Microrheology of Soft Materials: A Tracking-Free Determination of the Frequency-Dependent Loss and Storage Moduli. *Phys. Rev. Materials* **2017**, *1* (7), 073804. https://doi.org/10.1103/PhysRevMaterials.1.073804.

(42) Escobedo-Sánchez, M. A.; Segovia-Gutiérrez, J. P.; Zuccolotto-Bernez, A. B.; Hansen, J.; Marciniak, C. C.; Sachowsky, K.; Platten, F.; Egelhaaf, S. U. Microliter Viscometry Using

a Bright-Field Microscope: η-DDM. *Soft Matter* **2018**, *14* (34), 7016–7025. https://doi.org/10.1039/C8SM00784E.

(43) Martinez, V. A.; Schwarz-Linek, J.; Reufer, M.; Wilson, L. G.; Morozov, A. N.; Poon, W. C. K. Flagellated Bacterial Motility in Polymer Solutions. *PNAS* **2014**, *111* (50), 17771–17776. https://doi.org/10.1073/pnas.1415460111.

(44) Martinez, V. A.; Besseling, R.; Croze, O. A.; Tailleur, J.; Reufer, M.; Schwarz-Linek, J.; Wilson, L. G.; Bees, M. A.; Poon, W. C. K. Differential Dynamic Microscopy: A High-Throughput Method for Characterizing the Motility of Microorganisms. *Biophys. J.* **2012**, *103* (8), 1637–1647. https://doi.org/10.1016/j.bpj.2012.08.045.

(45) Reufer, M.; Martinez, V. A.; Schurtenberger, P.; Poon, W. C. K. Differential Dynamic Microscopy for Anisotropic Colloidal Dynamics. *Langmuir* **2012**, *28* (10), 4618–4624. https://doi.org/10.1021/la204904a.

(46) Wilson, L. G.; Martinez, V. A.; Schwarz-Linek, J.; Tailleur, J.; Bryant, G.; Pusey, P. N.; Poon, W. C. K. Differential Dynamic Microscopy of Bacterial Motility. *Phys. Rev. Lett.* **2011**, *106* (1), 018101. https://doi.org/10.1103/PhysRevLett.106.018101.

(47) Boucher, C.; St-Laurent, G.; Loignon, M.; Jolicoeur, M.; De Crescenzo, G.; Durocher, Y. The Bioactivity and Receptor Affinity of Recombinant Tagged EGF Designed for Tissue Engineering Applications Is Defined by the Nature and Position of the Tags. *Tissue Eng. Part A* **2008**, *14* (12), 2069–2077. https://doi.org/10.1089/ten.tea.2008.0037.

(48) Rahme, K.; Chen, L.; Hobbs, R. G.; Morris, M. A.; O'Driscoll, C.; Holmes, J. D. PEGylated Gold Nanoparticles: Polymer Quantification as a Function of PEG Lengths and Nanoparticle Dimensions. *RSC Adv.* **2013**, *3* (17), 6085–6094. https://doi.org/10.1039/C3RA22739A.

(49) Boon, J. P.; Nossal, R.; Chen, S.-H. Light-Scattering Spectrum Due to Wiggling Motions of Bacteria. *Biophys. J.* **1974**, *14* (11), 847–864.

(50) Song, L.; Falzone, N.; Vallis, K. A. EGF-Coated Gold Nanoparticles Provide an Efficient Nano-Scale Delivery System for the Molecular Radiotherapy of EGFR-Positive Cancer. *Int. J. Radiat. Biol.* **2016**, *92* (11), 716–723. https://doi.org/10.3109/09553002.2016.1145360.

(51) Yarden, Y.; Harari, I.; Schlessinger, J. Purification of an Active EGF Receptor Kinase with Monoclonal Antireceptor Antibodies. *J. Biol. Chem.* **1985**, *260* (1), 315–319.

(52) Liberelle, B.; Boucher, C.; Chen, J.; Jolicoeur, M.; Durocher, Y.; De Crescenzo, G. Impact of Epidermal Growth Factor Tethering Strategy on Cellular Response. *Bioconjug. Chem.* **2010**, *21* (12), 2257–2266. https://doi.org/10.1021/bc1002604.

(53) Nielsen, T. T.; Wintgens, V.; Amiel, C.; Wimmer, R.; Larsen, K. L. Facile Synthesis of β-Cyclodextrin-Dextran Polymers by "Click" Chemistry. *Biomacromolecules* **2010**, *11* (7), 1710–1715. https://doi.org/10.1021/bm9013233.

(54) Kinh, C. D.; Thien, T. V.; Hoa, T. T.; Khieu, D. Q. Interpretation of 1H-NMR Spectrum of Alginate by 1H-1H TOCSY and COSY Spectrum. *Viet. J. Chem.* **2007**, *45* (6), 772.

(55) Engler, A. C.; Lee, H.; Hammond, P. T. Highly Efficient "Grafting onto" a Polypeptide Backbone Using Click Chemistry. *Angew. Chem. Int. Ed.* **2009**, *48* (49), 9334–9338. https://doi.org/10.1002/anie.200904070.

(56) Patel, K. G.; Swartz, J. R. Surface Functionalization of Virus-Like Particles by Direct Conjugation Using Azide−Alkyne Click Chemistry. *Bioconjug. Chem.* **2011**, *22* (3), 376–387. https://doi.org/10.1021/bc100367u.

(57) Grant, G. T.; Morris, E. R.; Rees, D. A.; Smith, P. J. C.; Thom, D. Biological Interactions between Polysaccharides and Divalent Cations: The Egg-Box Model. *FEBS Lett.* **1973**, *32* (1), 195–198. https://doi.org/10.1016/0014-5793(73)80770-7.

(58) Ritger, P. L.; Peppas, N. A. A Simple Equation for Description of Solute Release II. Fickian and Anomalous Release from Swellable Devices. *J. Controlled Release* **1987**, *5* (1), 37–42. https://doi.org/10.1016/0168-3659(87)90035-6.

(59) Ritger, P. L.; Peppas, N. A. A Simple Equation for Description of Solute Release I. Fickian and Non-Fickian Release from Non-Swellable Devices in the Form of Slabs, Spheres, Cylinders or Discs. *J. Controlled Release* **1987**, *5* (1), 23–36. https://doi.org/10.1016/0168-3659(87)90034-4.

TABLE OF CONTENTS GRAPHIC

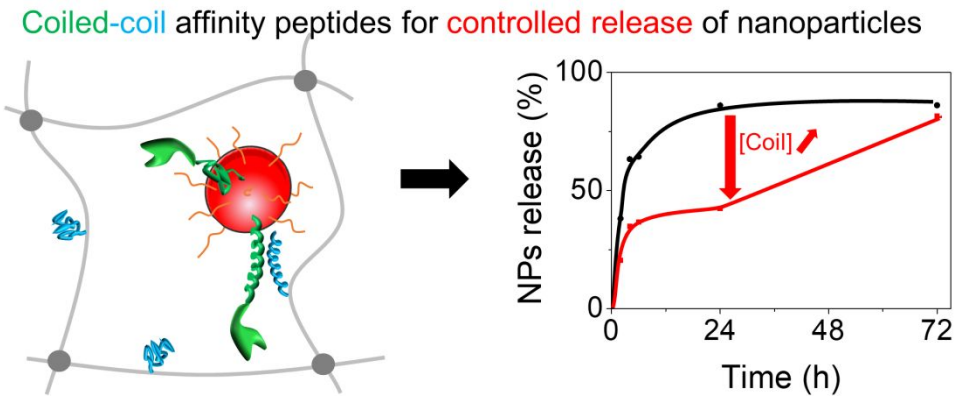

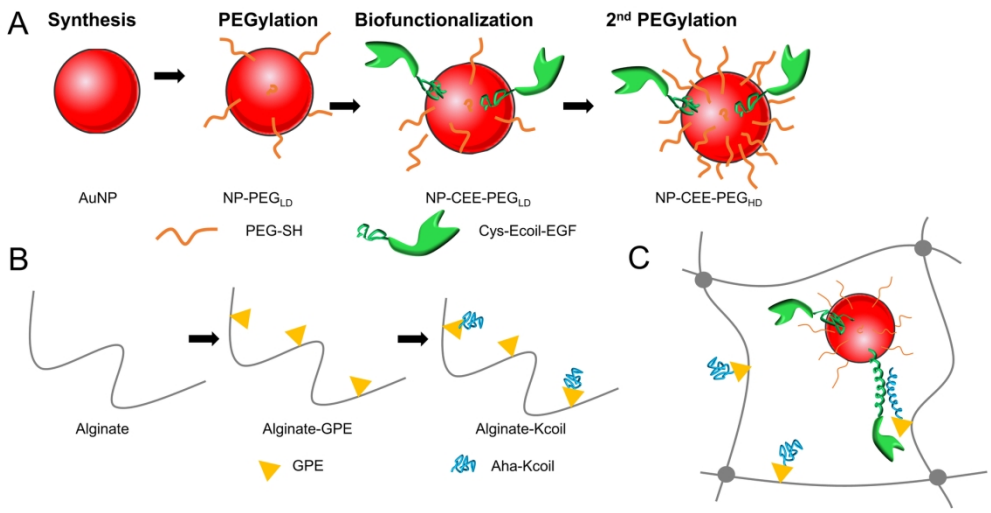

Figure 1. Preparation of the affinity-based hybrid system using gold nanoparticles and an alginate scaffold. (A) AuNPs were first PEGylated to a low level for stabilization. Cys-Ecoil-EGF (CEE) was then grafted via thiol-gold chemistry. A second PEGylation step was then performed for higher stability. (B) Alginate chains were first derivatized with an alkyne moiety using glycidyl propargyl ether (GPE). Azidohomoalanine-tagged Kcoil peptides (Aha-Kcoil) were then grafted via azide-alkyne click chemistry. (C) The dispersion of Ecoil-AuNPs in the Kcoil-alginate hydrogel enabled the formation of the E/K coiled-coil complex to slow down NPs release.

169x90mm (300 x 300 DPI)

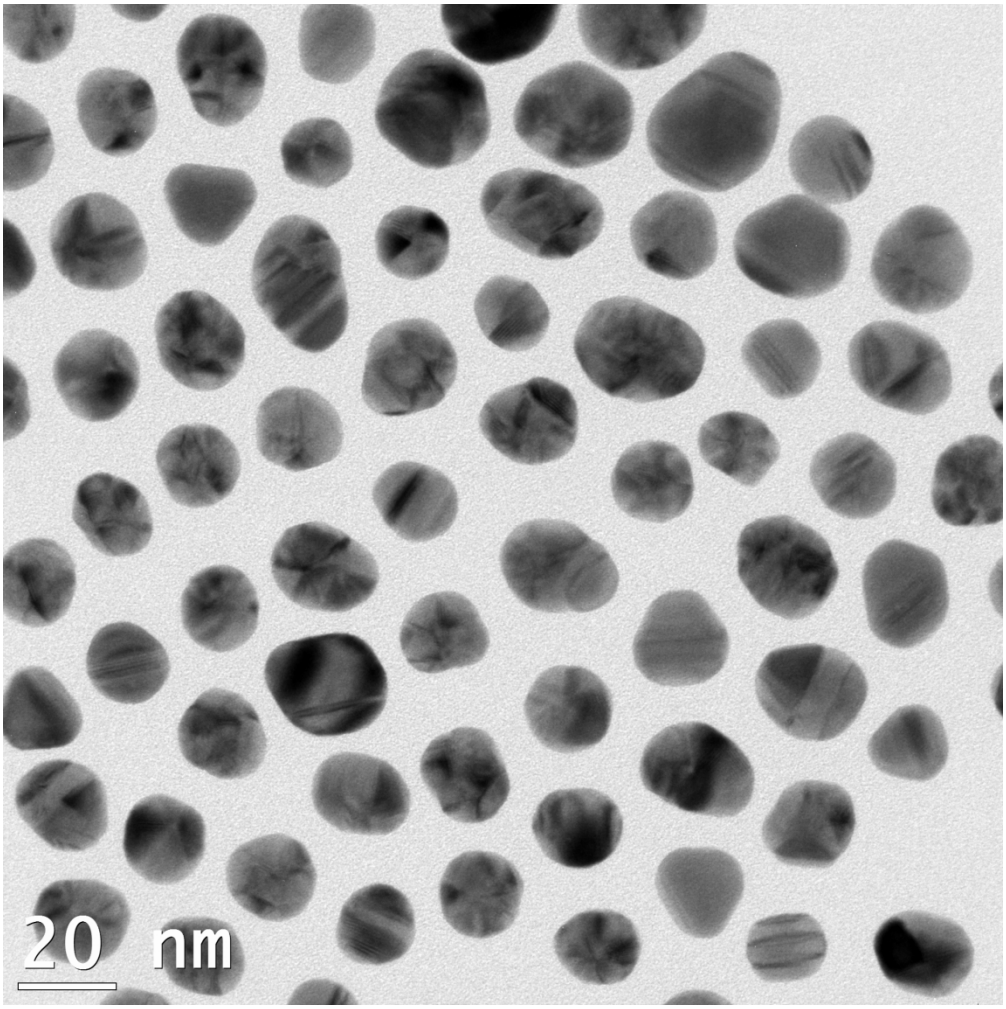

Figure 2 : Transmission electron microscopy (TEM) image of AuNPs.
The average NPs diameter measured was 18 ± 2 nm (n=100).

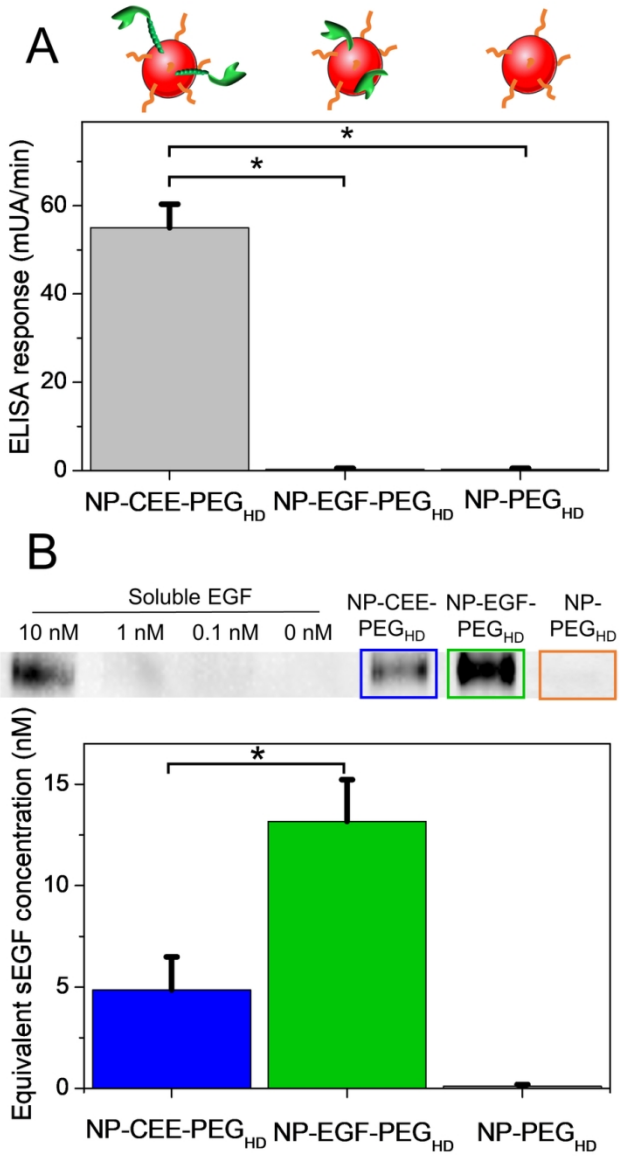

Figure 3. Bioadhesion and bioactivity of functionalized NPs.
(A) Bioadhesion on a Kcoil-derivatized surface of NP-CEE-PEGHD, NP-EGF-PEGHD, and NP-PEGHD as control, as detected by anti-EGF ELISA (n=3) (B) EGFR phosphorylation in A431 cells upon binding with soluble EGF (10, 1, 0.1 and 0 nM), NP-CEE-PEGHD or NP-EGF-PEGHD (EGF concentration of 1.5 nM according to ELISA) and NP-PEGHD , as monitored by Western Blot. The 180-kDa band immunoreactive to anti-phosphotyrosine antibodies (corresponding to EGFR) was quantified using a ChemiDoc and Image Lab software. Y-axis represents the equivalent concentration in soluble EGF (sEGF) (n = 3 for NP-CEE-PEGHD and NP-EGF-PEGHD and n = 1 for NP-PEGHD, * indicates statistical differences between datasets (bilateral t-test, $p < 0.05$).

82x149mm (300 x 300 DPI)

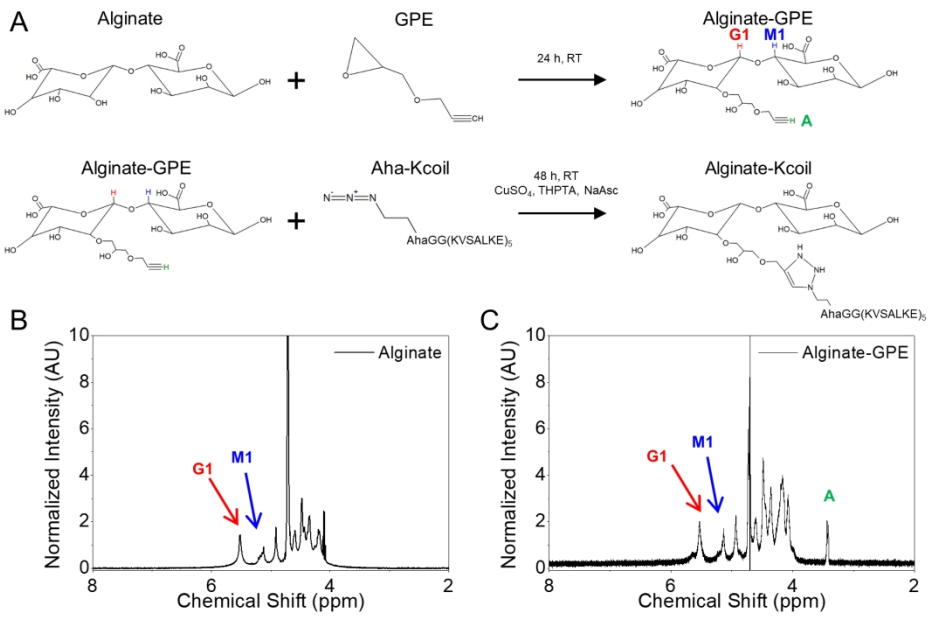

Figure 4. Synthesis and characterization of Kcoil-derivatized alginate.
(A) Alginate was first modified with glycidyl propargyl ether (GPE). Azide-terminated Kcoil peptides were then grafted on alginate-GPE via alkyne-azide click chemistry in presence of copper sulfate. (B and C) The percentage of alkyne-modified monomers was quantified by 1H NMR using the peak at 3.4 ppm (peak A), corresponding to the alkyne, and the peaks at 5.5 ppm (G1) and 5.1 ppm (M1) as reference, corresponding to the total amount of monomers.

170x104mm (300 x 300 DPI)

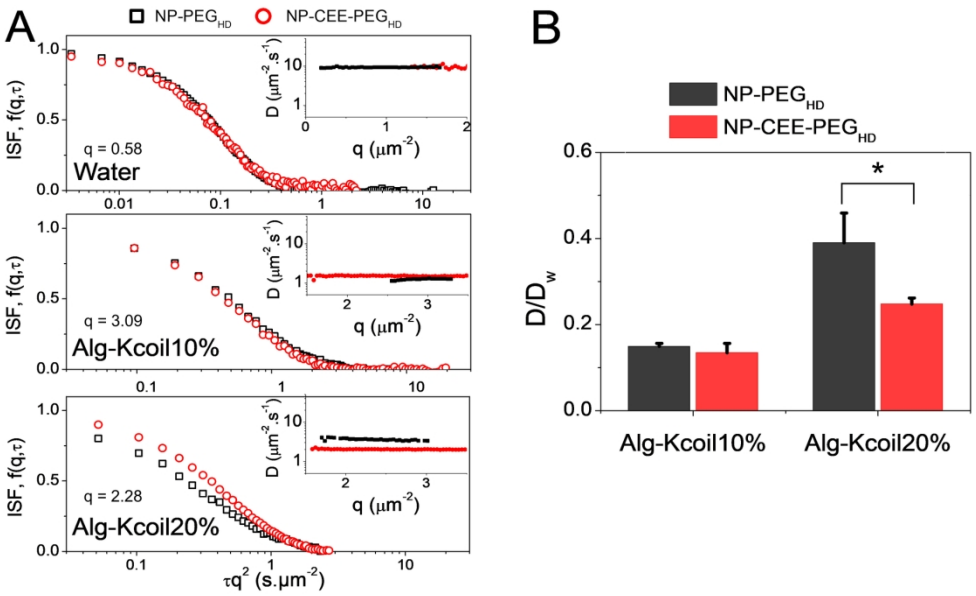

Figure 5. Diffusive properties of NPs assessed by differential dynamic microscopy. (A) Intermediate scattering function f(q,τ)=exp(-(τ/τR)β) of NP-CEE-PEGHD (red circles) and NP-PEGHD (black squares) in water, Alg-Kcoil10% and Alg-Kcoil20%. In Alg-Kcoil10%, ISF were calculated using a double exponential as in Eq.6. Insets represent the coefficient diffusion D (averaged from 5 videos) vs q for each type of NPs. Different q-values were used for each medium to best represent the short-time plateau and the long-time plateau of the ISF. (B) Diffusion coefficients of NP-CEE-PEGHD and NP-PEGHD, as determined by DDM. The Y-axis represents the ratio between the coefficients of diffusion of NPs in the hydrogels, D, and in water, Dw. * indicates statistical differences between datasets (n = 5) (bilateral t-test, $p < 0.05$).

170x104mm (300 x 300 DPI)

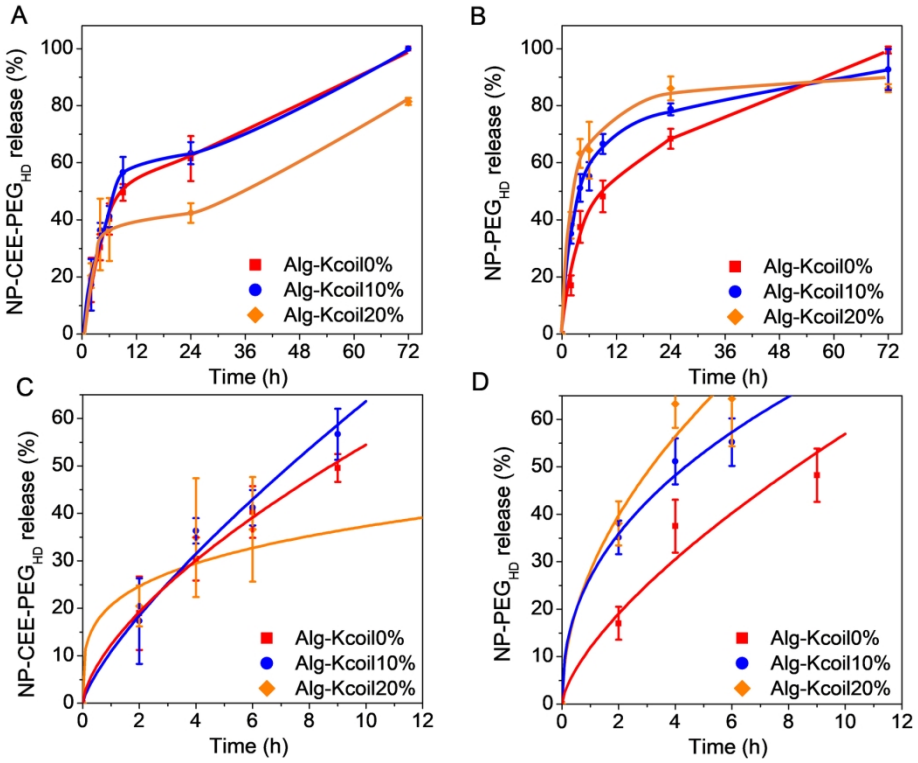

Figure 6. NPs release from Kcoil-modified alginate hydrogels. NP-CEE-PEGHD (A) and NP-PEGHD (B) are released from Alg-Kcoil0%, Alg-Kcoil10% and Alg-Kcoil20%, as calculated from the number of NPs still entrapped in the gel relative to t = 0. NP-CEE-PEGHD (C) and NP-PEGHD (D) data were fitted with a power-law model: each exponent was found to be between 0.43 and 1, characteristic of diffusion (both Fickian and non-Fickian), except for NP-CEE-PEGHD in Alg-Kcoil20%. (n≥4)

170x137mm (300 x 300 DPI)

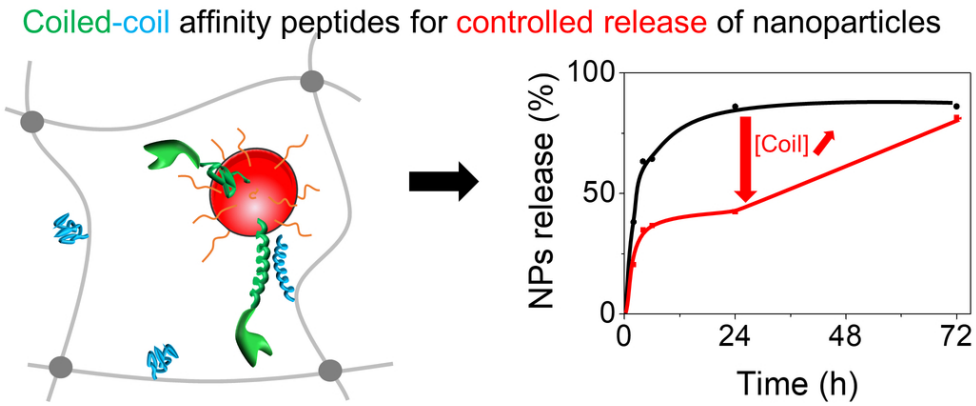

Graphic for Table of Content

88x35mm (300 x 300 DPI)